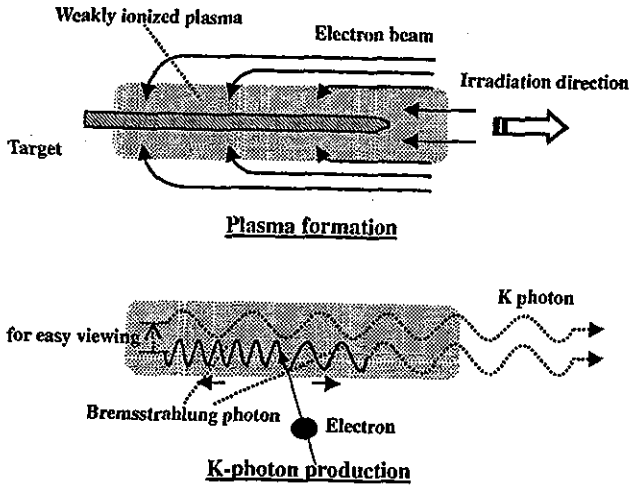

Fig. 3. K-photon irradiation from the plasma. The bremsstrahlung X-rays are absorbed and are converted into fluorescent (characteristic) X-rays in the weakly ionized linear plasma.

2.2. X-ray tube

The X-ray tube is a demountable cold cathode triode connected to a turbo-molecular pump. The pressure in the tube is approximately 1 mPa (Fig. 2). The tube consists of the following major parts: a hollow cylindrical carbon cathode with a bore diameter of 10.0 mm, a trigger electrode made from copper wire, a stainless steel vacuum chamber, a nylon insulator, a polyethylene terephthalate (Mylar) X-ray window 0.25 mm in thickness, and a rod-shaped nickel target 3.0 mm in diameter with a tip angle of 60°. The distance between the target and cathode electrodes is approximately 20 mm, and the trigger electrode is set in the cathode electrode. The electron beam from the cathode electrode is roughly focused onto the target by the electric field in the tube, and evaporation leads to the formation of a weakly ionized linear plasma of nickel ions and electrons around the fine target.

2.3. Principle of characteristic X-ray irradiation

In the linear plasma, bremsstrahlung photons with energies higher than the K-absorption edge are effectively absorbed and are converted into fluorescent X-rays (Fig. 3). The plasma then transmits the fluorescent rays easily, and bremsstrahlung rays with energies lower than the K-edge are also absorbed by the plasma. In addition, because bremsstrahlung rays are not emitted in the direction opposite that of electron acceleration, intense characteristic X-rays are generated along axial direction of the plasma.

3. Characteristics

3.1. Tube voltage and current

The tube voltage and current were measured by a high-voltage divider with an input impedance of 1 GΩ and a current transformer, respectively. Fig. 4 shows the time relation for the tube voltage and current. At the indicated charging voltages, they displayed damped oscillations. When the charging voltage was increased, both the maximum tube voltage and current increased. At a charging voltage of 50 kV, the maximum tube voltage was almost equal to the charging voltage of the main condenser, and the maximum tube current was approximately 17 kA.

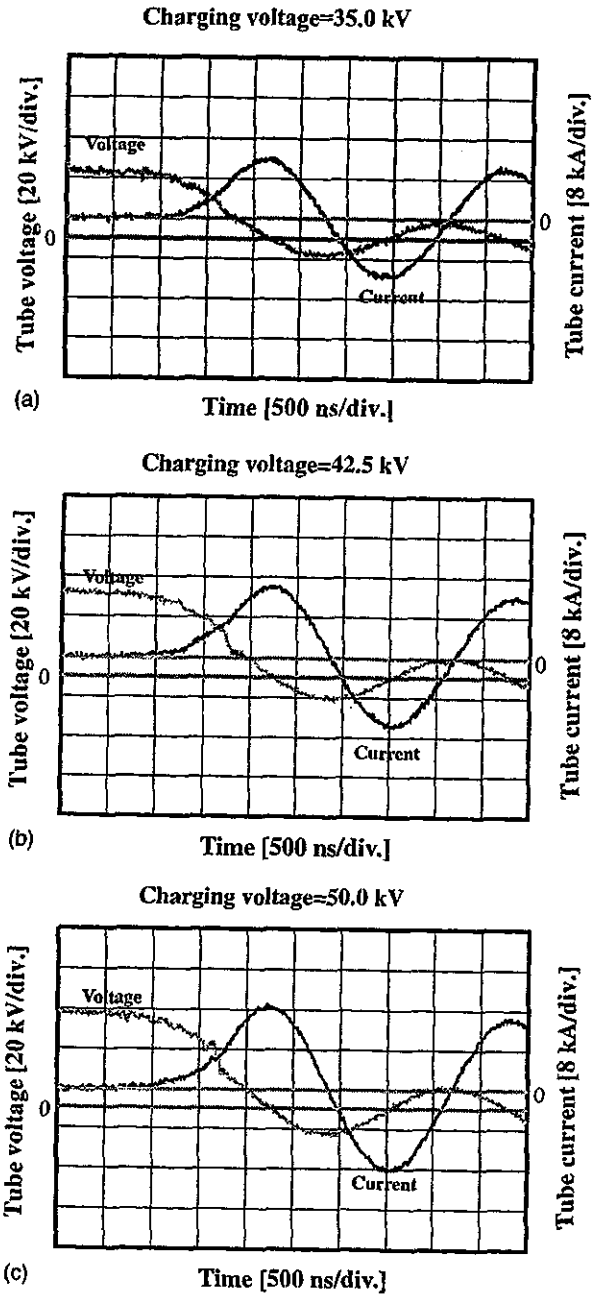

Fig. 4. Tube voltages and currents with a charging voltage of (a) 35.0, (b) 42.5, and (c) 50.0 kV.

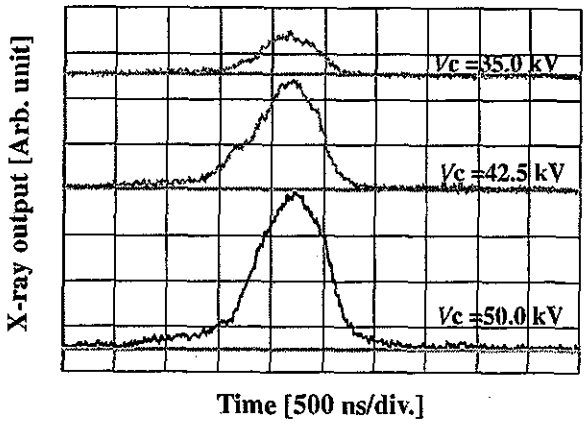

Fig. 5. X-ray outputs measured by a plastic scintillator with changes in the charging voltage.

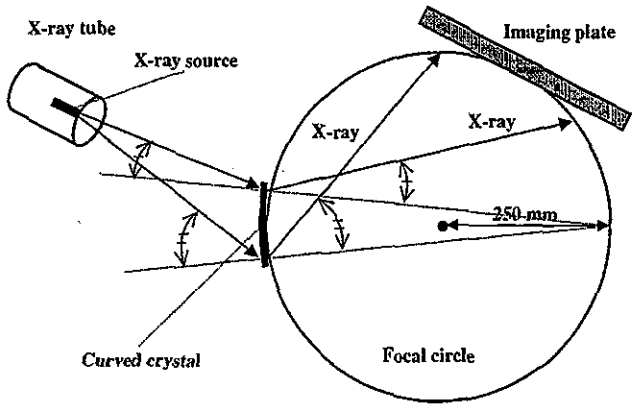

Fig. 7. Transmission-type spectrometer with a lithium fluoride curved crystal and an imaging plate. The X-rays from the source are diffracted by the crystal and are imaged by the imaging plate.

3.2. X-ray output

X-ray output pulse was detected using a combination of a plastic scintillator and a photomultiplier (Fig. 5). The X-ray pulse height substantially increased with corresponding increases in the charging voltage. The X-ray pulse widths were about 700 ns, and the time-integrated X-ray intensity per pulse, measured by a thermoluminescence dosimeter (Kyokko TLD Reader 1500 having MSO-S elements without energy compensation), had a value of about 30 μC/kg at 1.0 m from the X-ray source with a charging voltage of 50 kV.

3.3. X-ray source

The images of the plasma X-ray source were taken using a pinhole camera with a hole diameter of 100 μm (Fig. 6). When the charging voltage was increased, the plasma X-ray source grew, and both the beam dimension and the intensity increased.

3.4. X-ray spectra

X-ray spectra from the plasma source were measured by a transmission-type spectrometer (Fig. 7) with a lithium fluoride curved crystal of 0.5 mm in thickness. The spectra were taken by a computed radiography (CR) system (Konica Regius 150) [17] with a wide dynamic range, and the relative X-ray intensity was calculated from Dicom digital data. Fig. 8 shows measured spectra from the nickel target. We observed quite sharp lines of K-series characteristic X-rays such as lasers, while bremsstrahlung rays were hardly detected. The characteristic X-ray intensities of K_α and K_β lines substantially increased with corresponding increases in the charging voltage, and the K_β line was absorbed by a monochromatic cobalt filter of 15 μm thickness.

3.5. X-ray divergence

In order to ascertain the difference in characteristics between X-rays from a conventional tube and these from the

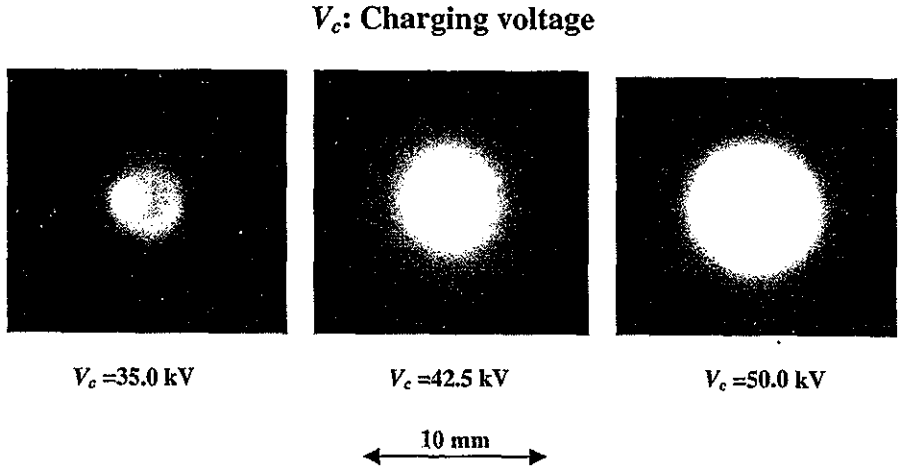

Fig. 6. Images of the plasma X-ray source measured by a pinhole of 100 μm from the plasma axial direction.

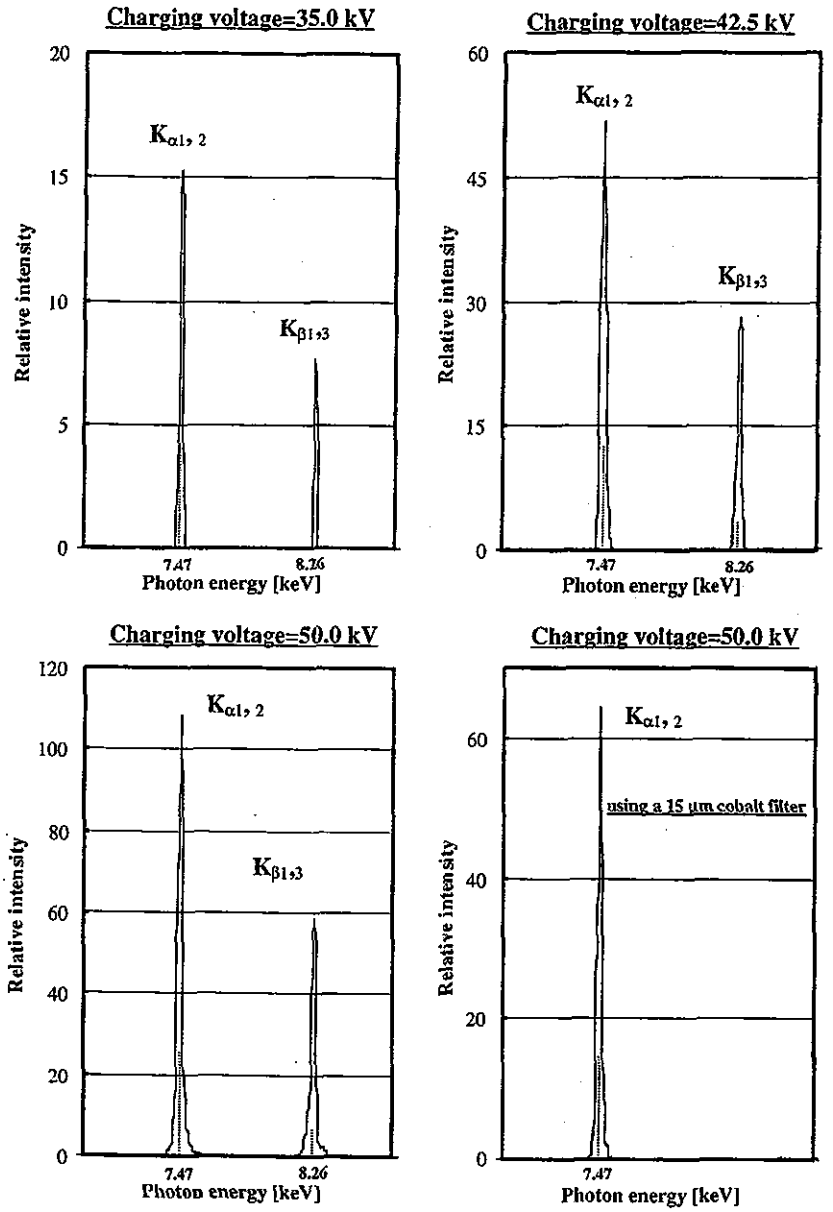

Fig. 8. X-ray spectra from weakly ionized nickel plasma according to changes in the charging voltage and to insertion of a cobalt monochromatic filter. In the measurement, we observed very sharp and intense characteristic X-rays such as lasers, while bremsstrahlung X-rays were hardly detected at all.

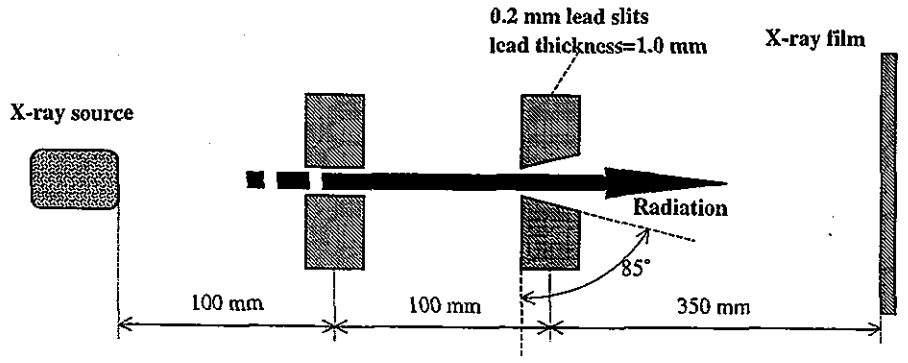

Fig. 9. Experimental setup for measuring X-ray divergence using two lead slits.

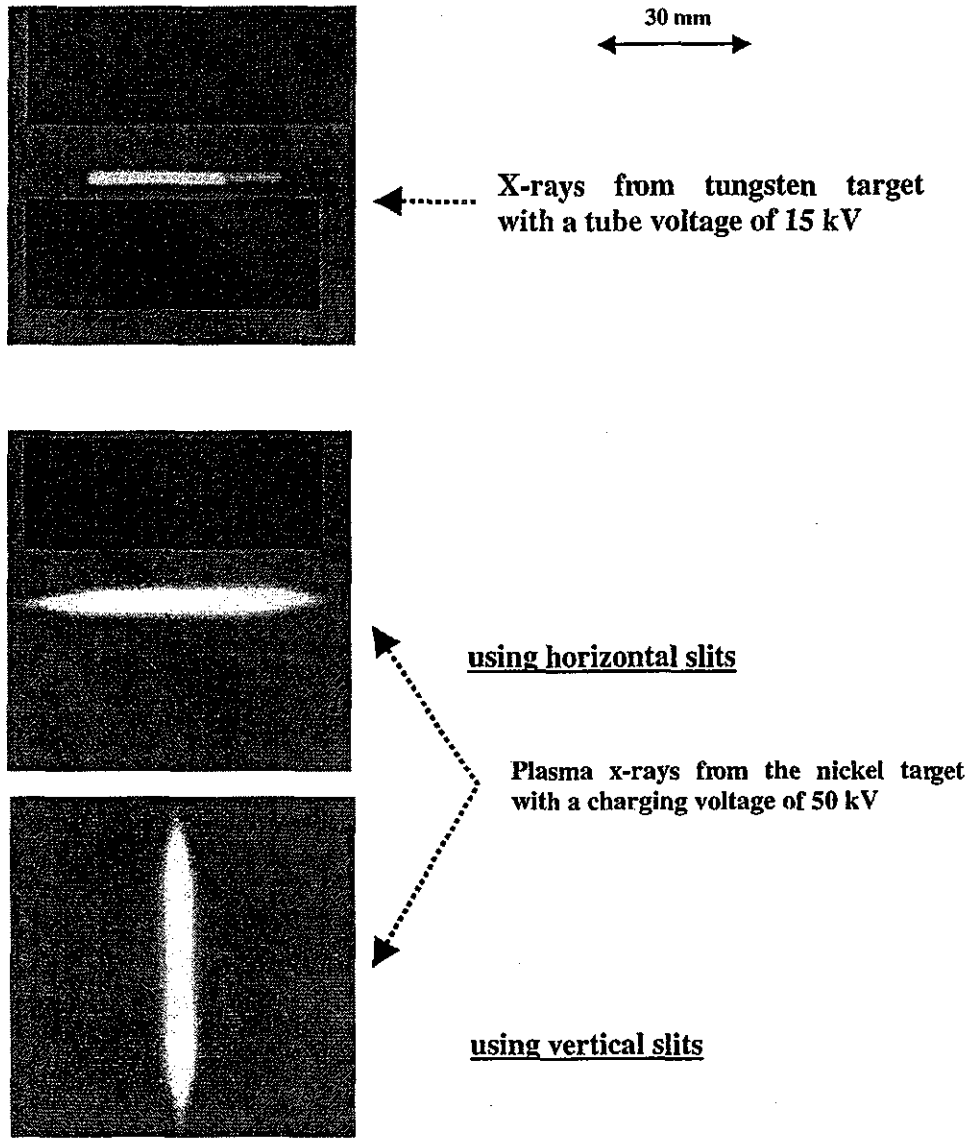

Fig. 10. X-ray divergence with two lead slits. The characteristic X-rays from the plasma were diffused greatly after passing through two lead slits.

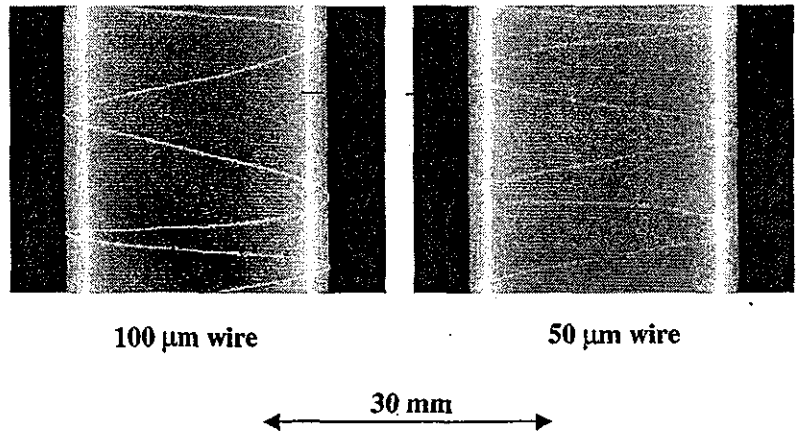

Fig. 11. Radiograms of tungsten wires of 50 and 100 μm in diameter coiled around pipes made of polymethyl methacrylate.

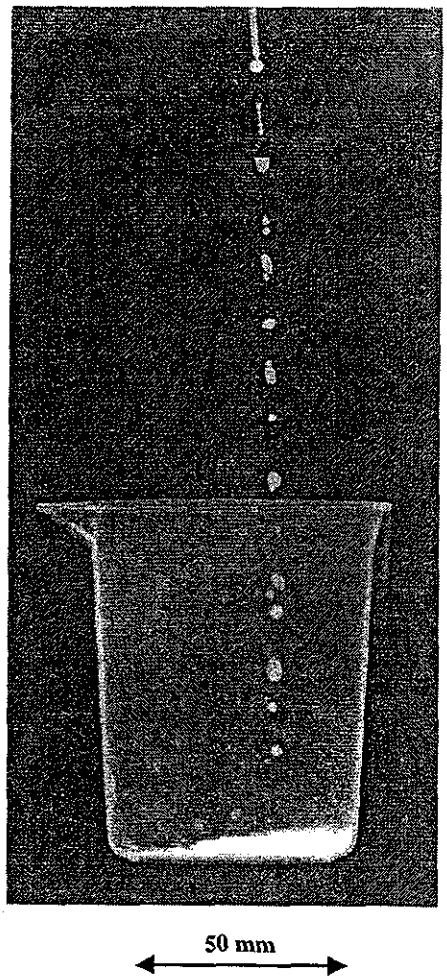

Fig. 12. Radiogram of water droplets falling into a polypropylene beaker from an injector.

plasma tube, we employed two lead slits in order to measure the divergence of the X-rays (Fig. 9). As compared with X-rays from a conventional tube with a tungsten target, the characteristic X-rays from the linear plasma were diffused greatly after passing through the two slits (Fig. 10).

4. Radiography

The plasma radiography was performed by the CR system (Konica Regius 150) without using a monochromatic filter, and the distance between the X-ray source and imaging plate was 1.2 m.

Firstly, the image resolution was measured using wires. Fig. 11 shows radiograms of tungsten wires coiled around pipes made of polymethyl methacrylate at a charging voltage of 50 kV. Although the image contrast increased with increases in the wire diameter, a 50 μm-diameter wire could be observed.

The image of water droplets falling into a polypropylene beaker from an injector is shown in Fig. 12. This image

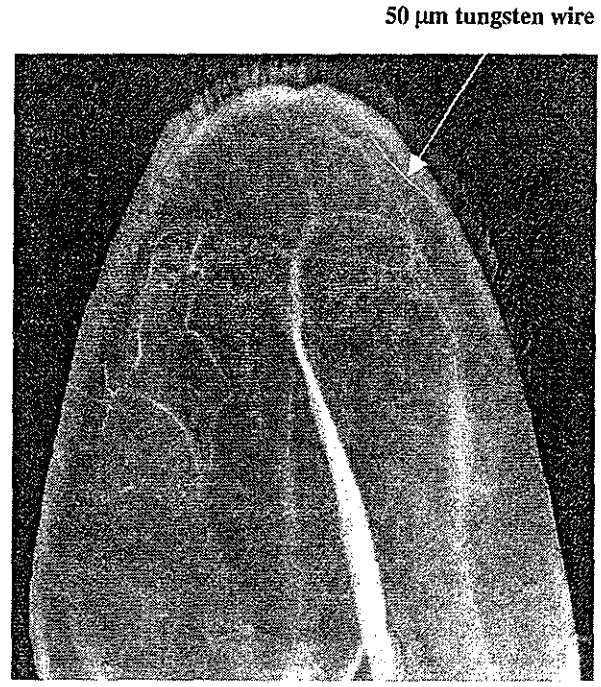

Fig. 13. Angiograms of the external ear of a rabbit.

was taken at a charging voltage of 45 kV, with the slight addition of an iodine-based contrast medium. Because the X-ray duration was about 1 μs, the stop-motion image of water could be obtained.

Fig. 13 shows an angiogram of the external ear of a rabbit; iodine-based microspheres of 15 μm diameter were used at a charging voltage of 45 kV, and fine blood vessels of about 50 μm were clearly visible.

5. Discussion

Regarding the spectrum measurement, although we obtained quite intense and sharp K-series lines without bremsstrahlung X-rays by forming a linear plasma X-ray source, we could not observe the difference between the $K\alpha_1$ and $K\alpha_2$ lines. In addition, we confirmed the divergence of K-series characteristic X-rays using two lead slits, and the maximum divergence angle was approximately 0.5°.

If we assume that the characteristic and bremsstrahlung X-rays are signal and noise, respectively, the signal to noise ratio is higher than 1000:1, and this value is almost equal to those of soft X-ray lasers produced by the gas-discharge capillary.

In this research, we obtained sufficient characteristic X-ray intensity per pulse for CR radiography, and the generator produced number of characteristic photons of approximately 1×10^{14} photons/cm^2 s at 1.0 m from the source. In addition, since the photon energy of characteristic X-rays can be controlled by changing target elements, various quasi-monochromatic high-speed radiographies,

such as high-contrast micro angiography[22] and parallel radiography[23] using an X-ray lens, will be possible.

Acknowledgements

This work was supported by Grants-in-Aid for Scientific Research and Advanced Medical Scientific Research from MECSST (12670902, 13470154, and 13877114), Grants from Keiryo Research Foundation, JST (Test of Fostering Potential), NEDO, and MHLW (HLSRG, RAMT-nano-001, RHGTEFB-genome-005, and RGCD13C-1).

References

[1] A. Mattsson, Physica Scripta 5 (1972) 99.
[2] R. Germer, J. Phys. E: Sci. Instrum. 12 (1979) 336.
[3] E. Sato, H. Isobe, F. Hoshino, Rev. Sci. Instrum 57 (1986) 1399.
[4] E. Sato, S. Kimura, S. Kawasaki, H. Isobe, K. Takahashi, Y. Tamakawa, T. Yanagisawa, Rev. Sci. Instrum. 61 (1990) 2343.
[5] A. Shikoda, E. Sato, M. Sagae, T. Oizumi, Y. Tamakawa, T. Yanagisawa, Rev. Sci. Instrum. 65 (1994) 850.
[6] E. Sato, K. Takahashi, M. Sagae, S. Kimura, T. Oizumi, Y. Hayasi, Y. Tamakawa, T. Yanagisawa, Med. Biol. Eng. Comput. 32 (1994) 289.
[7] K. Takahashi, E. Sato, M. Sagae, T. Oizumi, Y. Tamakawa, T. Yanagisawa, Jpn. J. Appl. Phys. 33 (1994) 4146.
[8] E. Sato, M. Sagae, A. Shikoda, K. Takahashi, T. Oizumi, M. Yamamoto, A. Takabe, K. Sakamaki, Y. Hayasi, H. Ojima, K. Takayama, Y. Tamakawa, SPIE 2869 (1996) 937.
[9] J.J. Rocca, V. Shlyaptsev, F.G. Tomasel, Phys. Rev. Lett. 73 (1994) 2192.
[10] G.P. Collins, Phys. Today 10 (1994) 19.
[11] J.J.G. Rocca, J.L.A. Chilla, S. Sakadzic, SPIE 4505 (2001) 1.
[12] S. Le Pape, P. Zeitoun, J.J.G. Rocca, SPIE 4505 (2001) 23.
[13] E. Sato, Y. Suzuki, Y. Hayasi, E. Tanaka, H. Mori, T. Kawai, K. Takayama, H. Ido, Y. Tamakawa, SPIE 4505 (2001) 154.
[14] E. Sato, Y. Hayashi, E. Tanaka, H. Mori, T. Kawai, H. Obara, T. Ichimaru, K. Takayama, H. Ido, T. Usuki, K. Sato, Y. Tamakawa, SPIE 4508 (2001) 176.
[15] E. Sato, Y. Hayasi, R. Germer, E. Tanaka, H. Mori, T. Kawai, H. Obara, T. Ichimaru, K. Takayama, H. Ido, Jpn. J. Med. Imag. Inform. Sci. 20 (2003) 148.
[16] E. Sato, Y. Hayasi, R. Germer, E. Tanaka, H. Mori, T. Kawai, H. Obara, T. Ichimaru, K. Takayama, H. Ido, Jpn. J. Med. Phys. 20 (2003) 123.
[17] E. Sato, K. Sato, Y. Tamakawa, Ann. Rep. Iwate Med. Univ. Sch. Lib. Arts Sci. 35 (2000) 13.

In Situ Measurements of Crossbridge Dynamics and Lattice Spacing in Rat Hearts by X-Ray Diffraction

Sensitivity to Regional Ischemia

James T. Pearson, PhD; Mikiyasu Shirai, MD, PhD; Haruo Ito, PhD; Noriyuki Tokunaga, MD; Hirotsugu Tsuchimochi, PhD; Naoki Nishiura; Daryl O. Schwenke, PhD; Hatsue Ishibashi-Ueda, MD; Ryuichi Akiyama, PhD; Hidezo Mori, MD, PhD; Kenji Kangawa, PhD; Hiroyuki Suga, MD, PhD; Naoto Yagi, PhD

Background—Synchrotron radiation has been used to analyze crossbridge dynamics in isolated papillary muscle and excised perfused hearts with the use of x-ray diffraction techniques. We showed that these techniques can detect regional changes in rat left ventricle contractility and myosin lattice spacing in in situ ejecting hearts in real time. Furthermore, we examined the sensitivity of these indexes to regional ischemia.

Methods and Results—The left ventricular free wall of spontaneously beating rat hearts (heart rate, 290 to 404 bpm) was directly exposed to brief high-flux, low-emittance x-ray beams provided at SPring-8. Myosin mass transfer to actin filaments was determined as the decrease in reflection intensity ratio (intensity of 1,0 plane over the 1,1 plane) between end-diastole and end-systole. The distance between 1,0 reflections was converted to a lattice spacing between myosin filaments. We found that mass transfer (mean, 1.71±0.09 SEM, n=13 hearts) preceded significant increases in lattice spacing (2 to 5 nm) during systole in nonischemic pericardium. Left coronary occlusion eliminated increases in lattice spacing and severely reduced mass transfer ($P<0.01$) in the ischemic region.

Conclusions—Our results suggest that x-ray diffraction techniques permit real-time in situ analysis of regional crossbridge dynamics at molecular and fiber levels that might also facilitate investigations of ventricular output regulation by the Frank-Starling mechanism. **(*Circulation*. 2004;109:2976-2979.)**

Key Words: ischemia ■ myocardial contraction ■ myosin ■ radiography

Despite the history of studies on crossbridge dynamics, lower photon counts and poorer quality of diffraction patterns obtained from cardiac muscle than skeletal and insect flight muscles[1–3] have limited progress with cardiac muscle until recently.[4,5] Some of us used third-generation synchrotron radiation (SPring-8, Japan Synchrotron Radiation Research Institute) to determine x-ray diffraction patterns in excised, perfused rat hearts while moving systematically across the left ventricular (LV) equator from the epicardium through to the ventricular cavity.[6]

X-ray diffraction patterns of cardiac muscle produce 2 equatorial-position reflections from the lattice-like arrangement of its protein elements.[2] Mass transfer of myosin heads to actin during contraction is inferred from a decrease in the integrated 1,0 reflection intensity ($I_{1,0}$, lattice plane containing only thick myosin filaments) and an increase in 1,1 reflection intensity ($I_{1,1}$, plane with thick myosin and thin actin filaments).[7] The myocardial intensity ratio (defined as $I_{1,0}/I_{1,1}$) is minimal in the rigor state and maximal in a quiescent state.[1,2,6,8]

Furthermore, the distance between 1,0 reflection peaks ($d_{1,0}$ spacing) represents the myosin lattice spacing, which is inversely related to sarcomere length in isolated fibers[5] as static myocytes maintain a constant cell volume. Whether decreases in myofilament spacing contribute to increasing Ca^{2+} sensitivity and increased probability of crossbridge formation at longer sarcomere lengths has been actively debated.[9] However, it is still not known if lattice spacing is regulated to maintain constant lattice volume (ie, if lattice cross-sectional area decreases with increasing sarcomere length, then interfilament spacing must decrease) during dynamic contractions in vivo.

Recently, it was shown that the intensity ratio derived from x-ray diffraction patterns of isolated whole hearts decreased during isovolumic contractions with a similar time course throughout the LV,[6] implying that crossbridge cycling in fibers of different myocardial layers is similar despite differences in fiber orientation and rate of short-

Received March 1, 2004; de novo received March 31, 2004; revision received May 6, 2004; accepted May 6, 2004.

From the National Cardiovascular Center Research Institute, Osaka, Japan (J.T.P., M.S., N.T., H.T., N.N., D.O.S., H.I.-U., H.M., K.K., H.S.); S-I Medico-Tech Co Ltd, Kashiwara, Osaka, Japan (H.I.); Muroran Institute of Technology, Muroran, Japan (R.A.); and SPring-8/JASRI, Sayo, Hyogo, Japan (N.Y.)

Correspondence to Dr James T. Pearson, Cardiac Physiology, National Cardiovascular Center Research Institute, 5-7-1 Fujishirodai, Suita, Osaka 565-8565 Japan. E-mail jpearson@ri.ncvc.go.jp

Circulation is available at http://www.circulationaha.org DOI: 10.1161/01.CIR.0000133322.19340.EF

ening. However, it was not possible to follow dynamic lattice spacing changes. In the present study, we used a fine-focused x-ray beam to record diffraction patterns of a localized region of the LV of ejecting rat hearts in situ and then determined crossbridge cycling and myosin lattice spacing.

Methods

Animals and Surgical Preparation

Anesthetized (50 mg/kg sodium pentobarbital IP) male Sprague-Dawley rats (Japan SLC, Hamamatsu, Japan), 9 to 10 weeks of age (350 to 400 g), were artificially ventilated and thoractomized. Procedures were performed according to SPring-8 guidelines for the care and welfare of experimental animals. The heart was continuously irrigated while the apex was raised by a manipulator paddle and restrained by 2 superficial sutures in the LV to minimize vertical movements. Pressure-volume loops were recorded from an apically inserted 1.4F micromanometer (SPR-671 Millar Instruments) and a 1.5F conductance catheter (S-I Medico-tech Co Ltd, Osaka)[10] to determine the temporal sequence of cardiac events and heart rate (determined from end-diastole [ED] interval).

X-Ray Diffraction With Collimated Synchrotron Radiation

Measurements were conducted at the *40XU beamline of SPring-8*.[6] A collimated quasimonochromatic beam (wavelength, 0.08 nm) with a beam flux of $\approx 10^{12}$ photons per second (15 keV; ring current, 60 to 100 mA) and dimensions 0.2 × 0.2 mm was focused at an oblique tangent to the myocardium (≈3 m from the detector). The ventilator was stopped at end-expiration to reduce heart movements during measurements (≈2.1 seconds). Images were digitally recorded at a 15-ms sampling interval with the use of an image intensifier and a fast CCD camera,[6] simultaneous with pressure-volume analog signals (1000-Hz sampling frequency). The beam passed through the apical myocardium between the ends of the descending branch of the left coronary artery (LAD) and the posterior interventricular vein. Final burning of the recorded region (higher energy levels) confirmed that the beam only exposed fibers in the epicardium and part of the intermediate layer (histological inspection).

Acute Ischemia Treatment

Heart baseline recordings were established, permanent ligation of the proximal LAD was performed, and recordings were repeated 5 to 10 minutes later.

Intensity Ratio Calculations and Analyses

Integrated intensity of $I_{1,0}$ and $I_{1,1}$ was determined from the areas under the reflection peaks after background subtraction.[6] Intensity ratio ($I_{1,0}/I_{1,1}$) was used rather than absolute reflection intensities of $I_{1,0}$ and $I_{1,1}$, which are influenced by changes in the quantity of fibers sampled during contractions.[5] Myosin mass transfer index was defined as the difference in intensity ratio between ED and end systole (ES).

Results

Mass Transfer and Lattice Spacing in Nonischemic Hearts

Intensity ratio significantly decreased during systole (increase in LV pressure [LVP] and decrease in LV volume [LVV]) and conversely, increased during diastole under the baseline rhythm (Figure 1a). Averaging intensity ratio over multiple beats reduced variability during diastole in the otherwise sinusoidal patterns (black lines, Figure 1b). With regard to time, $d_{1,0}$ spacing increased continuously during systole and then decreased during diastole, suggesting that considerable changes occur in the myofilament spacing (red line, Figure 1b).

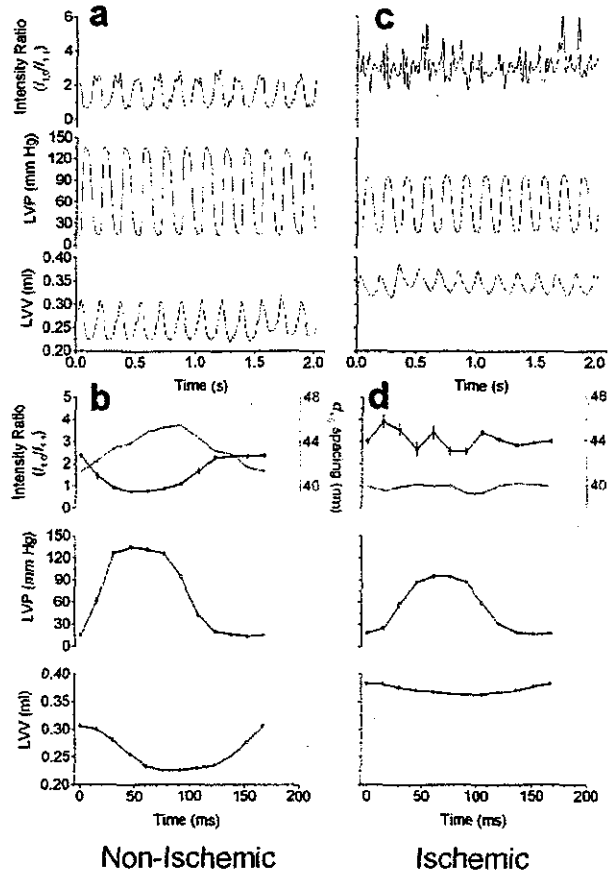

Figure 1. Relations between calculated intensity ratio, $d_{1,0}$ spacing, LVP, and LVV obtained from an LV with the use of x-ray diffraction. a and c, Consecutive records (15-ms intervals) of intensity ratio, LVP, and LVV during the baseline (a) and after LAD occlusion (c) in the same heart. b and d, Average changes in intensity ratio (black lines), $d_{1,0}$ spacing (red lines), LVP, and LVV over the cardiac cycle between the ED events (derived from a and c, respectively; bars indicate SEM).

Intensity ratio averaged 2.80±0.11 (SEM, n=13 hearts) at ED, and the average myosin mass transfer index was 1.71±0.09. In all hearts, the decrease in intensity ratio during crossbridge formation was completed before the full extent of the $d_{1,0}$ spacing change (2 to 5 nm between hearts, Figure 2a). Furthermore, at any given LVV, the $d_{1,0}$ spacing during systole was 1 to 2 nm larger than diastole (Figure 2b).

Mass Transfer and Lattice Spacing During Regional Ischemia

LAD occlusion reduced the intensity ratio change and prevented normal lattice spacing increase, consistent with reduced contractility of the ischemic region (Figure 1, c and d). Occlusion significantly increased intensity ratios at both ED ($P<0.05$) and ES ($P<0.001$) in the same LV region ($n=6$,

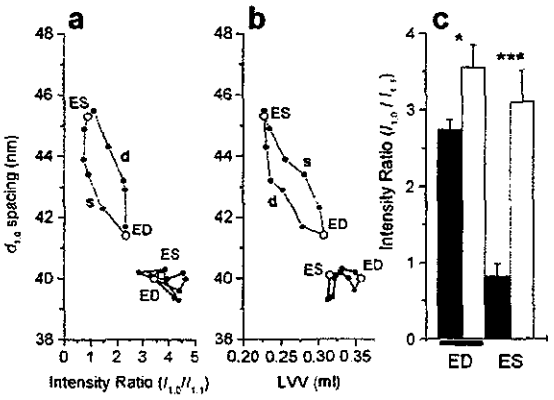

Figure 2. a and b, Average loops formed between $d_{1,0}$ spacing, LVV, and intensity ratio during consecutive cycles (shown in Figure 1) under baseline conditions (black symbols) and regional ischemia (red symbols). Systolic (s) and diastolic (d) trajectories are indicated for baseline. c, Mean intensity ratio at ED and ES during baseline (black columns) and regional ischemia (open columns; group mean±SEM). Ischemia versus baseline, paired *t* test **P*<0.05, ****P*<0.001.

Figure 2c). Although mean heart rate was not depressed (341±16 bpm, 4% increase) and there was only a small decrease in mean LV ES pressure (−26.9±5.8 mm Hg SEM), regional ischemia severely depressed the mass transfer index (55% of baseline).

Discussion

Our data clearly demonstrate that current synchrotron technology can produce sufficient energy to obtain well-defined reflections from single exposures to enable calculation of intensity ratio and $d_{1,0}$ spacing in in situ rat hearts (Figure 1). The mean ED intensity ratio of this study is similar to 2.96 obtained from LV in arrested rat hearts under normoxic perfusion.[8] Furthermore, in rat papillary muscles, the resting ratio was 3.07.[1,2] The results presented here were restricted to epicardial recordings (within 0.8-mm depth), consisting of helically orientated fibers, to minimize the contributions from fibers with orientations that vary at greater depth.[11] Nevertheless, it was recently established that neither diastolic intensity ratio nor mass transfer varies with depth of x-ray beam penetration in beating, perfused hearts (paced at 2 Hz).[6]

In Situ Changes in Myofilament Spacing

We showed that significant lattice expansion occurs during contraction and that the relation between $d_{1,0}$ spacing and intensity ratio is not linear but a loop in nonischemic hearts (black line, Figure 2a). The $d_{1,0}$ spacing changes during contraction (2 to 5 nm) were larger than the 1-nm difference in $d_{1,0}$ spacing reported between the epicardium and endocardium (at diastole).[6] Therefore, the larger $d_{1,0}$ spacing change found in ejecting hearts cannot be explained by shifts in the fiber layers exposed to the beam. The loop formed by these indexes might contain valuable information about how crossbridge axial and radial forces alter the dynamics of lattice spacing changes. Crossbridge projections from the myosin backbone produce radial force perpendicular to that of axial force in the filament direction.[12] Release of isometric tension in intact skeletal myofibers during sarcomere shortening causes a brief and rapid lattice spacing increase, in excess of that predicted by fiber shortening in itself.[12,13] We therefore conclude that lattice volume is not constant in the dynamic state because myosin lattice spacing is significantly larger (1 to 2 nm) during contraction than ventricular filling at the same LVV ($d_{1,0}$ spacing during systole greater than diastole, Figure 2b). Crossbridge formation probably causes a brief lattice expansion in ejecting hearts mediated by radial forces.

Sensitivity of In Situ Indexes to Regional Ischemia

The relevance of our new findings is that although the intensity ratio of beating hearts in diastole was similar to that of relaxed papillary muscles, there is a very different response of the myocardium in beating hearts to ischemia in terms of crossbridge dynamics and lattice space changes. Higher intensity ratios and more variable intensity ratio changes during systole (Figure 1, c and d) occurred as the result of lower absolute $I_{1,1}$ in systole and a lack of consistent increase in $I_{1,1}$ when $I_{1,0}$ decreased (data not shown). Thus, permanent regional ischemia severely attenuated mass transfer in the epicardium (Figure 2c). Furthermore, ischemia induced increases in ED intensity ratio in vivo, whereas other studies report maximal decreases in the intensity ratio under anoxic perfusion (isolated arrested hearts)[8] or rigor.[1,2] An increase in intensity ratio might be related to metabolite accumulation or pronounced passive stretching, because fiber shortening in infarcted regions progressively decreases until fibers eventually become passively stretched (bulging) by fiber shortening in the nonischemic region.[14] In support of the bulging possibility, we found that $d_{1,0}$ spacing no longer increases between ED and ES after occlusion.

The cellular basis of the Frank-Starling law of the heart involves increases in contractility caused by length-dependent increases in Ca^{2+} sensitivity associated with increased ventricular filling.[9] However, it is still debated whether increased crossbridge activation results from increased probability of crossbridge formation with decreasing lattice spacing associated with fiber stretching (see review in Reference 9). In a future publication, we will examine how LV volume loading influences mass transfer in relation to myofilament spacing and length-dependent activation of contraction in situ.

Acknowledgments

This work was supported by the Promotion of Fundamental Studies in Health Sciences of the Organization for Pharmaceutical Safety and Research (OPSR) and Ministerial grants Nano-001 and a Grant-in-Aid for Scientific Research. The experiments were made with approval of the SPring-8 Program Review Committee. We thank Dr Keiji Umetani for access to the Medical Imaging Center.

References

1. Matsubara I, Kamiyama A, Suga H. X-ray diffraction study of contracting heart muscle. *J Mol Biol*. 1977;111:121–128.
2. Matsubara I, Suga H, Yagi N. An X-ray diffraction study of the cross-circulated canine heart. *J Physiol (London)*. 1977;270:311–320.

3. Yagi N, Saeki Y, Ishikawa T, et al. *Cross-bridge and calcium behavior in ferret papillary muscle in different thyroid states. Jpn J Physiol.* 2001;51:319–326.
4. Konhilas JP, Irving TC, de Tombe PP. Myofilament calcium sensitivity in skinned rat cardiac trabeculae: role of interfilament spacing. *Circ Res.* 2002;90:59–65.
5. Irving TC, Konhilas J, Perry D, et al. Myofilament lattice spacing as a function of sarcomere length in isolated rat myocardium. *Am J Physiol.* 2000;279:H2568–H2573.
6. Yagi N, Shimizu J, Mohri S, et al. *X-ray diffraction from a left* ventricular wall of rat heart. *Biophys J.* 2004;86:2286–2294.
7. Huxley HE, Brown W. The low-angle x-ray diagram of vertebrate striated muscle and its behaviour during contraction and rigor. *J Mol Biol.* 1967;30:383–434.
8. Sowerby AJ, Harries J, Diakun GP, et al. X-ray diffraction studies of whole rat heart during anoxic perfusion. *Biochem Biophys Res Commun.* 1994;202:1244–1251.
9. Konhilas JP, Irving TC, de Tombe PP. Frank-Starling law of the heart and the cellular mechanisms of length-dependent activation. *Pflugers Arch.* 2002;445:305–310.
10. Ito H, Takaki M, Yamaguchi H, et al. Left ventricular volumetric conductance catheter for rats. *Am J Physiol.* 1996;270:H1509–H1514.
11. Streeter DD Jr, Spotnitz HM, Patel DP, et al. *Fiber orientation in the* canine left ventricle during diastole and systole. *Circ Res.* 1969;24: 339–347.
12. Cecchi G, Bagni MA, Griffiths PJ, et al. Detection of radial cross-bridge force by lattice spacing changes in intact single muscle fibers. *Science.* 1990;250:1409–1411.
13. Bagni M, Cecchi G, Griffiths P, et al. Lattice spacing changes accompanying isometric tension development in intact single muscle fibers. *Biophys J.* 1994;67:1965–1975.
14. Lew WYW, Chen Z, Guth B, et al. Mechanisms of augmented segment shortening in nonischemic areas during acute ischemia of the canine left ventricle. *Circ Res.* 1985;56:351–358.

ELSEVIER

Cardiovascular Research 64 (2004) 125–131

Cardiovascular Research

www.elsevier.com/locate/cardiores

Extraneuronal enzymatic degradation of myocardial interstitial norepinephrine in the ischemic region

Takafumi Fujii[a], Toji Yamazaki[a,*], Tsuyoshi Akiyama[a], Shunji Sano[b], Hidezo Mori[a]

[a] *Department of Cardiac Physiology, National Cardiovascular Center Research Institute, 5-7-1 Fujishiro-dai, Suita, Osaka 565-8565, Japan*
[b] *Department of Cardiovascular Surgery, Okayama University Medical School, Okayama 700-8558, Japan*

Received 19 March 2004; received in revised form 28 May 2004; accepted 14 June 2004
Available online 22 July 2004
Time for primary review 26 days

Abstract

Objective: Catechol *O*-methyltransferase (COMT) is believed to exert degradative action at high norepinephrine (NE) levels. Although COMT exists in cardiac tissues, the contribution of cardiac COMT activity to regional NE kinetics, particularly in ischemia-induced NE accumulation, remains unclear. We investigated the role of cardiac COMT in NE kinetics in the ischemic region. **Methods:** We implanted a microdialysis probe into the left ventricular myocardium of anesthetized rabbits and induced myocardial ischemia by 60-min coronary artery occlusion. We monitored myocardial interstitial levels of NE and its metabolites in the presence and absence of a COMT inhibitor. We intraperitoneally administered entacapone (10 mg/kg) 120 min before control sampling. **Results:** In control, entacapone increased interstitial dihydroxyphenylglycol (DHPG, intraneuronal NE metabolite by monoamine oxidase (MAO)) levels and decreased interstitial normetanephrine (NMN, extraneuronal NE metabolite by COMT) and 3-methoxy-4-hydroxyphenylglycol (MHPG, extraneuronal DHPG metabolite by COMT) levels, but did not change interstitial NE levels. Coronary occlusion increased NE levels to 165 ± 48 nM at 45–60 min of occlusion. This increase was accompanied by increases in DHPG and NMN levels (11.3 ± 1.1 and 9.3 ± 1.3 nM at 45–60 min of occlusion). Entacapone augmented the ischemia-induced NE and DHPG responses (333 ± 51 and 22.9 ± 2.4 nM at 45–60 min of occlusion). In contrast, the ischemia-induced NMN response was suppressed by entacapone (2.0 ± 0.4 nM at 45–60 min of occlusion). Reperfusion decreased interstitial NE levels and increased interstitial DHPG and NMN levels. Entacapone suppressed changes in NE and NMN levels, but augmented the increase in dialysate DHPG. **Conclusion:** Myocardial ischemia evoked increases in myocardial interstitial NE and NMN levels. COMT inhibition augmented the increase in NE (substrate of COMT) levels and suppressed the increase in NMN (metabolite by COMT) levels. In the ischemic heart, COMT contributes to the removal of accumulated NE in the myocardium.

Keywords: Adrenergic agonists; Autonomic nervous system; Ischemia; Reperfusion; Neurotransmitters

1. Introduction

It has been reported that myocardial ischemia evokes an excessive norepinephrine (NE) accumulation in the myocardial interstitial space [1,2]. Outward NE transport through the uptake$_1$ carrier has been proposed as an important mechanism responsible for this ischemia-induced NE accumulation [2–4]. The presence of such high NE levels in the myocardial interstitium may be involved in the progression of myocardial cell injury and a higher incidence of malignant arrhythmia [5,6].

In the non-ischemic heart, released NE is reclaimed by cardiac sympathetic nerve endings via the uptake$_1$ carrier and repackaged or metabolized to dihydroxyphenylglycol (DHPG) by monoamine oxidase (MAO). NE, which escapes the synapses to the myocardial interstitium, spills over into the bloodstream or is taken up by extraneuronal cells via the uptake$_2$ carrier and mainly degraded to NE metabolites by catechol *O*-methyltransferase (COMT) [6–9] (Fig. 1). In the ischemic heart, normal transport by the uptake$_1$ carrier is impaired and NE spills over into the bloodstream, which is decreased due to the reduction of myocardial blood flow [1]. Therefore, extraneuronal enzymatic degradation may be the only mechanism that decreases myocardial interstitial NE. Little information, however, is available on the extraneuronal NE degradation by COMT in the ischemic region [10,11].

* Corresponding author. Tel.: +81-6-6833-5012x2380; fax: +81-6-6872-8092.
E-mail address: yamazaki@ri.ncvc.go.jp (T. Yamazaki).

0008-6363/$ - see front matter © 2004 European Society of Cardiology. Published by Elsevier B.V. All rights reserved.
doi:10.1016/j.cardiores.2004.06.011

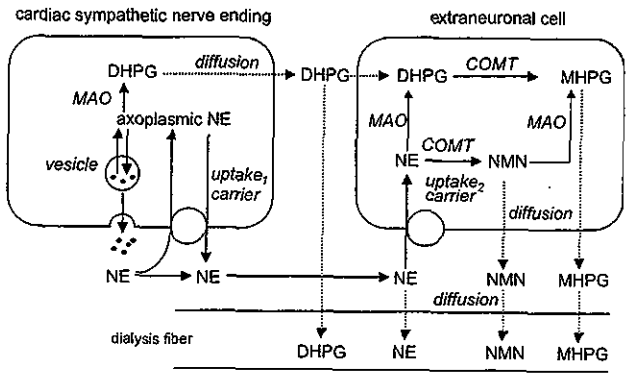

Fig. 1. Schema of putative factors affecting norepinephrine (NE) degradation in the cardiac sympathetic nerve ending and the extraneuronal cell. COMT, catechol *O*-methyltransferase; DHPG, dihydroxyphenylglycol; MAO, monoamine oxidase; NMN, normetanephrine; MHPG, 3-methoxy-4-hydroxyphenylglycol.

Until now, available methodology for examination of organ-specific NE degradation has been limited to the assessment of radiolabelled-catecholamine kinetics [12]. Previously, using the dialysis technique in the in vivo heart, we demonstrated that coronary occlusion evokes a marked increase of myocardial interstitial NE levels in the ischemic region [1,2,4] and that outward NE transport through the uptake$_1$ carrier is involved in this NE efflux [2–4]. Moreover, we recently reported that the dialysis technique makes it possible to simultaneously monitor interstitial levels of NE and extraneuronal metabolites in the rabbit skeletal muscle [13]. Therefore, we consider it possible to elucidate extraneuronal NE metabolism and the role of COMT in its metabolism in the ischemic region. In the present study, we applied the dialysis technique to the heart of anesthetized rabbits and investigated myocardial interstitial levels of NE and its extraneuronal metabolites during coronary occlusion and reperfusion and examined the effect of COMT blockade on myocardial interstitial levels of NE and its metabolites.

2. Methods

2.1. Animal preparation

The investigation conformed with the Guide for the Care and Use of Laboratory Animals published by the US National Institutes of Health (NIH Publication No. 85-23, revised 1996). Adult male Japanese white rabbits (2.5–3.2 kg) were anesthetized with pentobarbital sodium (30–35 mg/kg iv). The level of anesthesia was maintained with a continuous intravenous infusion of pentobarbital sodium (1–2 mg/kg/h). The rabbits were intubated and ventilated with room air mixed with oxygen. Body temperature was maintained at around 38 °C with a heating pad and lamp. Heart rate, arterial pressure, and electrocardiogram were monitored and recorded continuously. Heparin sodium (200 IU/kg) was first administered intravenously and then maintained with a continuous infusion (5–10 IU/kg/h) to prevent blood coagulation. With the animal in the lateral position, the fifth or sixth rib on the left side was partially removed to expose the heart. A small incision was made in the pericardium, and the dialysis probe was implanted in the region perfused by the left circumflex coronary artery (LCX) of the left ventricular wall. A snare was placed around the main branch of LCX to act as the occluder for later coronary occlusion. To ensure that the sampling area was in the ischemic region, we examined the color and motion of the ventricular wall during a brief occlusion and confirmed that the dialysis probe was correctly located. To avoid a preconditioning effect, the duration of occlusion was limited to within seconds.

2.2. Dialysis technique

Materials suitable for cardiac dialysis probes have been described in detail elsewhere [14]. Briefly, we designed a handmade long transverse dialysis probe. One end of a polyethylene tube (25-cm length, 0.5 mm OD, and 0.2 mm ID) was dilated with a 27-gauge needle (0.4 mm OD). Each end of the dialysis fiber (8-mm length, 0.31 mm OD, and 0.20 mm ID; PAN-1200 50 000 molecular weight cutoff, Asahi Chemical Japan) was inserted into the polyethylene tube and glued. We used a fine guiding needle (30-mm length, 0.51 mm OD, and 0.25 mm ID) for implantation of the dialysis probes. We connected a guiding needle to a dialysis probe with a stainless rod (5-mm length and 0.25 mm OD). At perfusion speed of 2 μl/min, in vitro recovery rates of NE, DHPG, normetanephrine (NMN), and 3-methoxy-4-hydroxyphenylglycol (MHPG) were 46 ± 8%, 48 ± 1%, 33 ± 3%, and 46 ± 2%, respectively (number of dialysis probes = 3) [15].

Dialysis probes were perfused with Ringer's solution at a speed of 2 μl/min using a microinjection pump (Carnegie Medicine CMA/100). Ringer's solution consisted of (in mM) 147.0 NaCl, 4.0 KCl, 2.25 $CaCl_2$. Sampling periods were 30 min (1 sampling volume = 60 μl) in control and 15 min (1 sampling volume = 30 μl) during occlusion and reperfusion. Each sample was collected in a microtube containing 3 μl of 0.1 N HCl to prevent amine oxidation. Based on the results of our previous study [1,2], we commenced the protocol followed by a stabilization period of 2 h. Taking into consideration the dead space between the dialysis fiber and sample tube, we sampled the dialysate.

Dialysate NE, DHPG, NMN, and MHPG concentrations were measured as indices of myocardial interstitial NE, DHPG, NMN, and MHPG levels. Furthermore, dialysate NE and DHPG were used as indices of COMT substrate, and dialysate NMN and MHPG as indices of COMT production. We used three distinct systems of high-performance liquid chromatography (HPLC) with electrochemical detection for the highly sensitive measurements: one for NE, one for DHPG, and one for NMN and MHPG measurement [16–18]. The mobile phase consisted of 1-octane-sulfonic acid sodium salt in phosphate buffer and methanol. In each HPLC system, the concentration of each component and the reference voltage were adjusted to the optimum condition. One-

third each of the dialysate sample was used for the measurement of NE, DHPG, and NMN and MHPG. Dialysate NE concentration was measured by the first HPLC after removing interfering compounds by the alumina procedure [14,16]. Dialysate DHPG concentration was measured by direct injection into the second HPLC [17]. Dialysate NMN and MHPG concentrations were measured by direct injection into the third HPLC [18]. The detection limits of NE, DHPG, NMN, and MHPG were 0.2, 0.2, 1, and 0.9 pg/injection.

2.3. Experimental protocols

After control sampling, we occluded the main branch of LCX for 60 min and then released the occluder. We continuously sampled dialysate from the ischemic region during 60 min of coronary occlusion and 15 min of reperfusion.

2.3.1. Vehicle group (n=8)

We administered saline intraperitoneally as vehicle 120 min before control sampling. After control sampling, we observed the time course of dialysate NE, DHPG, NMN, and MHPG levels from the ischemic region during 60 min of coronary occlusion and 15 min of reperfusion.

2.3.2. Entacapone group (n=8)

To elucidate role of COMT in the ischemia-induced changes in myocardial interstitial NE and its metabolites, we observed the effect of COMT inhibitor on dialysate NE, DHPG, NMN, and MHPG levels in the ischemic region. We administered intraperitoneally a COMT inhibitor entacapone (10 mg/kg; Orion Parma, Espoo, Finland) 120 min before control sampling. Entacapone was dissolved in phosphate-buffered saline, the pH of the solution was adjusted to 7.4. The route and dose of entacapone were selected to cause the full inhibition of soluble COMT in tissue [19]. After control sampling, we observed the time course of dialysate NE, DHPG, NMN, and MHPG levels with a similar protocol to that used in the vehicle group.

At the end of each experiment, the rabbits were killed with an overdose of pentobarbital sodium, and the implant regions were checked to confirm that the dialysis probes had been implanted within the cardiac muscle.

2.4. Statistical analysis

Hemodynamic and dialysate NE, DHPG, MHPG, and NMN responses to coronary occlusion in the presence and absence of COMT inhibitor were statistically analyzed by two-way analysis of variance with repeated measures on one factor [20]. When a statistically significant effect of coronary occlusion was detected as a whole, the Newman–Keuls test was applied to determine which mean values differed significantly from each other. When statistically significant effect of the COMT inhibitor was detected, the Newman–Keuls test was applied to determine which periods differed significantly between the vehicle and entacapone groups. Statistical significance was defined as $P<0.05$. Values are presented as means ± SE.

3. Results

3.1. Time course of heart rate and arterial pressure

The time course of heart rate and mean arterial pressure is shown in Table 1. In the vehicle group, heart rate decreased after 15 min of occlusion, whereas in the entacapone group, heart rate increased after 30 min of occlusion. There was, however, no significant difference in heart rate between groups.

Coronary occlusion significantly decreased mean arterial pressure in both groups. In the entacapone group, mean arterial pressure was higher than those in the vehicle group at each sampling point, while changes in mean arterial pressure were similar to those in the vehicle group.

3.2. Dialysate NE levels in the ischemic region

Coronary occlusion significantly altered dialysate NE levels (Fig. 2). In the vehicle group, dialysate NE levels were 0.39 ± 0.07 nM in the control and increased after coronary occlusion. During 60 min of coronary occlusion, dialysate NE levels markedly increased and reached 165 ± 48 nM at 45–60 min of occlusion. After reperfusion, dialysate NE levels decreased to 62 ± 40 nM, although their

Table 1
Time course of heart rate and mean arterial pressure during coronary occlusion and reperfusion

	Control	Coronary occlusion (min)				Reperfusion (min)
		15	30	45	60	15
Heart rate (bpm)						
Vehicle group ($n=8$)	252 ± 6	236 ± 7*	238 ± 7*	239 ± 6*	237 ± 6*	238 ± 6*
Entacapone group ($n=8$)	246 ± 8	246 ± 8	251 ± 9*	253 ± 7*	253 ± 8*	251 ± 9
Mean arterial pressure (mm Hg)						
Vehicle group ($n=8$)	83 ± 3	71 ± 4*	75 ± 3*	76 ± 3*	78 ± 2*	76 ± 3*
Entacapone group ($n=8$)	99 ± 4†	85 ± 4*,†	88 ± 5*,†	88 ± 4*,†	88 ± 4*,†	86 ± 4*,†

Values are means ± SE.
* $P<0.05$ vs. control value.
† $P<0.05$ vs. concurrent value of vehicle group.

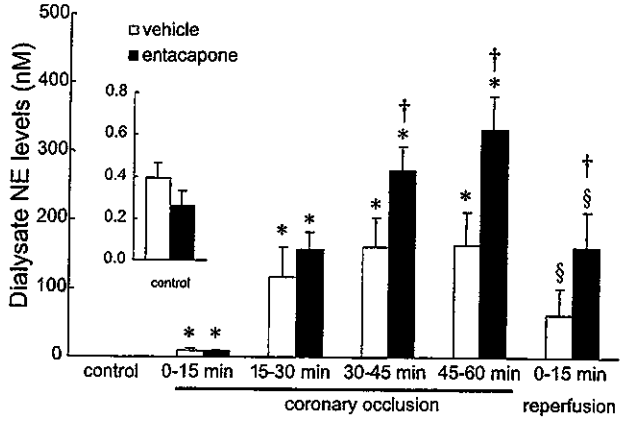

Fig. 2. Dialysate norepinephrine (NE) levels in the ischemic region. Values are means ± SE. *$P<0.05$ vs. control value, §$P<0.05$ vs. value at 45–60 min of occlusion, †$P<0.05$ vs. concurrent value of vehicle group.

levels were higher than those in the control. In the presence of entacapone, dialysate NE levels also markedly increased and reached 333 ± 51 nM at 45–60 min of occlusion. These increases in dialysate NE levels after 30 min of coronary occlusion were significantly enhanced by entacapone whereas entacapone did not change dialysate NE levels in the control (0.26 ± 0.07 nM). After reperfusion, dialysate NE levels decreased but remained higher than those in the vehicle group.

3.3. Dialysate DHPG levels in the ischemic region

Coronary occlusion significantly altered dialysate DHPG levels (Fig. 3). In the vehicle group, dialysate DHPG levels were 6.5 ± 0.5 nM in the control and did not change within 30 min of coronary occlusion. After 30 min of occlusion, dialysate DHPG levels gradually increased and reached 11.3 ± 1.1 nM at 45–60 min of occlusion. After reperfusion, dialysate DHPG levels further increased to 29.5 ± 2.6 nM. In the presence of entacapone, dialysate DHPG levels gradually increased during the ischemia and reached 22.9 ± 2.4 nM at 45–60 min of occlusion. After reperfusion, dialysate DHPG levels further increased to 52.6 ± 8.4 nM. In the presence of entacapone, dialysate DHPG levels in the control (9.9 ± 0.8 nM) and after reperfusion were higher than those in the vehicle group.

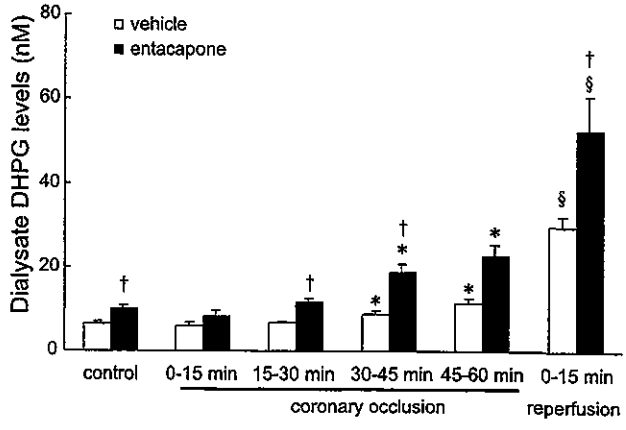

Fig. 3. Dialysate dihydroxyphenylglycol (DHPG) levels in the ischemic region. Values are means ± SE. *$P<0.05$ vs. control value, §$P<0.05$ vs. value at 45–60 min of occlusion, †$P<0.05$ vs. concurrent value of vehicle group.

3.4. Dialysate NMN levels in the ischemic region

Coronary occlusion significantly altered dialysate NMN levels (Fig. 4). In the vehicle group, dialysate NMN levels were 2.9 ± 0.4 nM in the control and increased after 30 min of occlusion and reached 9.3 ± 1.3 nM at 45–60 min of occlusion. After reperfusion, dialysate NMN levels further increased (11.9 ± 2.0 nM). Entacapone decreased dialysate NMN levels in the control to undetectable levels. Then dialysate NMN levels increased after 30 min of occlusion and reached 2.0 ± 0.4 nM at 45–60 min of occlusion. After reperfusion, dialysate NMN levels further increased to 4.1 ± 0.8 nM. Their NMN levels were lower than those in the vehicle group at each sampling point before, during, and after coronary occlusion.

3.5. Dialysate MHPG levels in the ischemic region

Coronary occlusion significantly altered dialysate MHPG levels (Fig. 5). In the vehicle group, dialysate MHPG levels were 3.9 ± 0.3 nM in the control. Dialysate MHPG levels transiently decreased 15–30 min after occlusion (3.6 ± 0.4 nM), but recovered after 30 min of occlusion. After reperfusion, dialysate MHPG levels increased to 5.5 ± 0.3 nM. Entacapone substantially decreased dialysate MHPG levels in the control (1.5 ± 0.4 nM). In the presence of entacapone, dialysate MHPG levels further decreased during occlusion and reached 0.6 ± 0.2 nM at 30–45 min of occlusion. After reperfusion, dialysate MHPG levels increased to 2.3 ± 0.5 nM. Their MHPG levels were lower than those in the

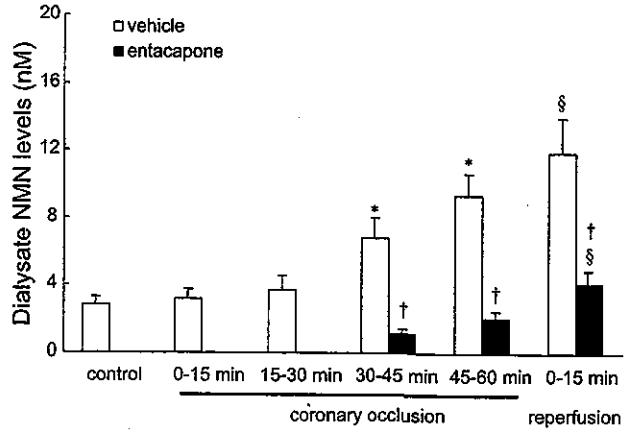

Fig. 4. Dialysate normetanephrine (NMN) levels in the ischemic region. Values are means ± SE. *$P<0.05$ vs. control value, §$P<0.05$ vs. value at 45–60 min of occlusion, †$P<0.05$ vs. concurrent value of vehicle group.

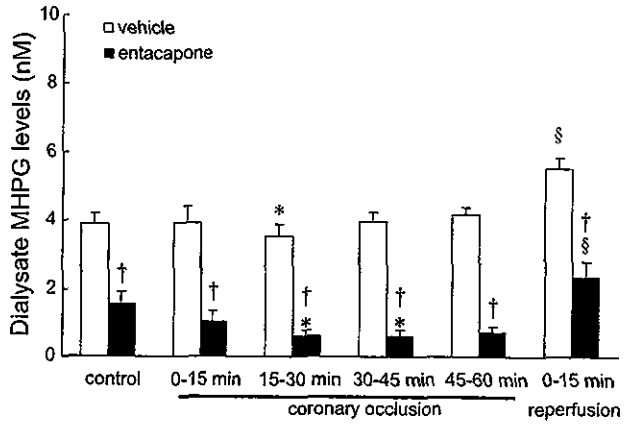

Fig. 5. Dialysate 3-methoxy-4-hydroxyphenylglycol (MHPG) levels in the ischemic region. Values are means ± SE. *$P<0.05$ vs. control value, §$P<0.05$ vs. value at 45–60 min of occlusion, †$P<0.05$ vs. concurrent value of vehicle group.

vehicle group at each sampling point before, during, and after coronary occlusion.

4. Discussion

Using the dialysis technique in the in vivo rabbit heart, we observed myocardial interstitial levels of NE and its neuronal and extraneuronal metabolites in the ischemic region and examined the contribution of extraneuronal NE degradation by COMT to myocardial interstitial NE levels. Our data demonstrate that COMT plays an important role in NE metabolism during 60 min of coronary occlusion and reperfusion.

4.1. Myocardial interstitial NE and its metabolites under control conditions

The administration of entacapone did not alter myocardial interstitial NE levels in the control. Degradation of NE by COMT may play a minor role in the changes in myocardial NE levels [21]. In general, NE that is taken up by cardiac sympathetic nerve endings is repackaged or metabolized to DHPG by MAO. On the other hand, NE that is taken up via extraneuronal NE transport systems by extraneuronal cells is metabolized to NMN or MHPG by COMT [7–10,22,23] (Fig. 1). In the present study, entacapone increased DHPG in the myocardial interstitium but did not alter myocardial interstitial NE levels in the control. Myocardial interstitial levels of DHPG were about 16-fold higher than those of NE and about 2- to 3-fold higher than those of NMN in the control. Therefore, under physiological conditions, released NE could be largely taken up by cardiac sympathetic nerve endings via the $uptake_1$ carrier and transferred into stored vesicle or metabolized to DHPG by MAO. A smaller percentage of released NE, which escapes the synapses, is taken up by extraneuronal cells via the $uptake_2$ carrier and is metabolized to NMN by COMT. Compared with MAO, COMT could play a minor role on the degradation of released NE in the control.

After entacapone administration, increases in myocardial interstitial DHPG accompanied decreases in myocardial interstitial MHPG levels in the control. These metabolites of NE penetrate the cell membrane by diffusion [24]. Their values serve as indices of the neuronal and extraneuronal NE metabolism. COMT blockade suppressed the degradation of DHPG to MHPG. Therefore, the decrease in MHPG levels and increase in interstitial DHPG levels could be ascribed to inhibition of COMT by entacapone. In rabbit heart, we confirmed the existence of COMT activity with the main substrate of COMT being DHPG rather than NE.

4.2. Myocardial interstitial NE and its metabolites during coronary occlusion

Myocardial interstitial NE levels markedly increased after 15 min of occlusion. In this phase, outward transport of NE via the $uptake_1$ carrier takes place from cardiac sympathetic nerve endings [2,3]. The marked increase in myocardial interstitial NE could be due to this non-exocytotic NE release and inhibition of neuronal reuptake via the $uptake_1$ carrier [2–4].

Entacapone augmented increases in myocardial interstitial NE levels after 30 min of coronary occlusion. This result indicates that COMT contributes to the degradation of myocardial interstitial NE in this phase. Neuronal reuptake via the normal mode of $uptake_1$ is dependent on the sodium gradient between the intra- and extraneuronal space [25]. Neuronal degradation of released NE via neuronal uptake cannot be expected in this phase because of a reduced sodium gradient [3,25]. Moreover, NE spillover into the bloodstream is decreased due to reduced myocardial blood flow [1]. On the other hand, extraneuronal NE uptake operates independently of the sodium gradient [26]. Burgdorf et al. [27] demonstrated that the extraneuronal monoamine transporter is activated during metabolic distress such as low flow ischemia. Previous investigations with similar preparations suggested that ketamine augments ischemia-induced NE accumulation by inhibition of extraneuronal uptake [28,29]. We consider that substantial NE in the myocardial interstitium is taken up alternatively by extraneuronal cells via the $uptake_2$ carrier and is metabolized to NMN by COMT in this phase. Thus, COMT activity plays an important physiological role in NE degradation in the ischemic period.

Myocardial interstitial NMN levels increased after 30 min of occlusion. Entacapone decreased basal myocardial interstitial NMN levels and suppressed the ischemia-induced increase in myocardial interstitial NMN levels. This suppression is consistent with the finding that COMT contributes to the degradation of myocardial interstitial NE via extraneuronal NE uptake. Furthermore, even in the presence of entacapone, myocardial interstitial NMN levels increased after 30 min of occlusion. An increase in interstitial NE levels may overcome the inhibition of COMT by

entacapone. Although COMT could play a minor role in the degradation of released NE in the control, a substantial increase in myocardial NE may cause the high affinity of the extraneuronal COMT system. In the control period, an extraneuronal COMT system may contribute to DHPG degradation, whereas in the ischemic period, both neuronal NE uptake and MAO activities may be suppressed by ischemia and alternatively the extraneuronal COMT system may promote NE degradation based on the fact that the myocardial interstitial NE levels in the ischemic period were 10-fold higher than those of DHPG. Therefore, we consider that increases in myocardial interstitial NE levels shift the main substrate of COMT from DHPG to NE.

The relationship between DHPG and MHPG supports our interpretation. In the control, entacapone increased myocardial interstitial DHPG levels and decreased myocardial interstitial MHPG levels. In contrast, in the ischemic period, increases in myocardial interstitial DHPG levels were not associated with increases in myocardial MHPG levels, but increases in myocardial NE levels accompanied increases in myocardial NMN. Thus, both DHPG and NE are metabolized by the extraneuronal COMT system, but the amount of NMN and MHPG may be dependent on the concentration of their substrate. Thus, there was a clear difference in the main metabolite by COMT between the non-ischemic and ischemic periods. The main metabolite by COMT was NMN rather than MHPG in the latter [30]. These results are limited to ischemia within 60 min because prolonged ischemia accompanies the structural membrane defects, and other mechanisms for NE release and degradation may be involved [31].

4.3. Myocardial interstitial NE and its metabolites after reperfusion

Myocardial interstitial NE levels decreased after reperfusion although they were higher than those in control. On the other hand, myocardial interstitial DHPG levels increased after reperfusion. The uptake$_1$ carrier resumes normal transport function after reperfusion [2,4]. The inward NE transport via the uptake$_1$ carrier could contribute to the decrease in myocardial interstitial NE levels. The increase in axoplasmic NE by uptake and the recovery of MAO activity could increase myocardial interstitial DHPG levels [2]. Thus, neuronal degradation by MAO contributes to decreasing myocardial interstitial NE after reperfusion.

Reperfusion caused a decrease in myocardial interstitial NE levels and an increase in myocardial NMN levels, both of which changes were suppressed by administration of entacapone. During the early reperfusion period, COMT activity promotes the degradation of NE. Myocardial interstitial NE levels were higher than those in the control. Therefore, during the ischemic and reperfusion periods, these higher NE levels in myocardial interstitium may serve as an effective substrate of COMT for NE degradation via extraneuronal NE uptake.

During the reperfusion period, increases in myocardial interstitial DHPG accompanied increases in myocardial interstitial MHPG levels. Furthermore, administration of entacapone suppressed both of these changes. Myocardial interstitial DHPG levels were similar to myocardial interstitial NE levels. These data suggest that COMT activity promotes the degradation of DHPG. Alternatively, higher NE level in myocardial interstitium may produce MHPG via COMT activity. Recently, we demonstrated in rabbit skeletal muscle that local administration of higher NE increased dialysate NMN but not MHPG levels, whereas local administration of higher DHPG increased dialysate MHPG levels [19]. Therefore, higher NE and DHPG levels serve as the substrate of COMT and independently yield NMN and MHPG during the reperfusion period. Thus, COMT activity plays an important physiological role in the reperfusion period.

4.4. Methodological considerations

In the presence of a high concentration of entacapone, mean arterial pressure was higher than that in the vehicle group at each sampling point before, during, and after coronary occlusion, but changes in mean arterial pressure were similar to those in the vehicle group. In the previous and present studies, intraperitoneal administration of entacapone did not alter control dialysate NE levels from skeletal muscle and myocardium [19]. In humans, entacapone did not alter plasma catecholamine levels or hemodynamics at rest or during exercise [32]. The influence of entacapone on pressure-regulating peptides remains unclear. An increase in mean arterial blood pressure might decrease dialysate NE levels through a baroreflex mechanism. Furthermore, baroreflex-independent and non-exocytotic NE efflux leads to high NE levels in the myocardial interstitium of ischemic regions, making it unlikely that hemodynamic change contributes to the removal of accumulated NE during myocardial ischemia.

Two major classes of COMT have been defined on the basis of their location: a soluble, cytosolic form and a membrane-bound form [33]. Entacapone inhibits both classes of COMT. The soluble, cytosolic form is generally assumed to be the predominant form of the enzyme. The membrane-bound form has been suggested to be responsible for O-methylation at low and physiologically relevant concentrations of the catecholamine neurotransmitters, whereas the soluble, cytosolic form predominates under conditions that lead to saturation of the membrane-bound form [33]. In the present study, myocardial interstitial norepinephrine levels reached 100–1000 times the normal plasma concentrations after 15 min of occlusion. Thus, a soluble, cytosolic form could contribute to the observed decrease in myocardial interstitial NE levels in the ischemic region.

5. Conclusion

Under physiological condition, extraneuronal enzymatic degradation by COMT plays a minor role on the inactivation

of myocardial interstitial NE. Under ischemic conditions, however, myocardial interstitial NE levels are markedly increased by ischemia. Normal transport by the uptake$_1$ carrier is impaired and NE spillover into the bloodstream is decreased due to the reduction of myocardial blood flow, but extraneuronal enzymatic degradation by COMT contributes to the decrease in myocardial interstitial NE levels in the ischemic region.

Acknowledgements

This work was supported by Grants-in-Aid for scientific research (15590787) from the Ministry of Education, Culture, Sports, Science and Technology; the Research Grants for Cardiovascular Disease (H13C-1) from the Ministry of Health, Labor and Welfare. The authors thank Orion-Pharma (Espoo, Finland) for the supply of entacapone.

References

[1] Akiyama T, Yamazaki T, Ninomiya I. Differential regional responses of myocardial interstitial noradrenaline levels to coronary occlusion. Cardiovasc Res 1993;27:817–22.
[2] Akiyama T, Yamazaki T. Myocardial interstitial norepinephrine and dihydroxyphenylglycol levels during ischemia and reperfusion. Cardiovasc Res 2001;49:78–85.
[3] Schömig A, Dart AM, Dietz R, Mayer E, Kübler W. Release of endogenous catecholamines in the ischemic myocardium of the rat. Part A: locally mediated release. Circ Res 1984;55:689–701.
[4] Shindo T, Akiyama T, Yamazaki T, Ninomiya I. Regional myocardial interstitial norepinephrine kinetics during coronary occlusion and reperfusion. Am J Physiol 1996;270:H245–51.
[5] Penny WJ. The deleterious effects of myocardial catecholamines on cellular electrophysiology and arrhythmias during ischaemia and reperfusion. Eur Heart J 1984;5:960–73.
[6] Waldenström AP, Hjalmarson AC, Thornell L. A possible role of noradrenaline in the development of myocardial infarction. Am Heart J 1978;95:43–51.
[7] Boulton AA, Eisenhofer G. Catecholamine metabolism. From molecular understanding to clinical diagnosis and treatment. Adv Pharmacol 1998;42:273–92.
[8] Grohmann M, Trendelenburg U. The substrate specificity of uptake2 in the rat heart. Naunyn Schmiedebergs Arch Pharmacol 1984;328: 164–73.
[9] Obst OO, Rose H, Kammermeier H. Characterization of catecholamine uptake2 in isolated cardiac myocytes. Mol Cell Biochem 1996;163–164:181–3.
[10] Inoue M, Hifumi K, Kurahashi K, Fujiwara M. Impairment of the extraneuronal O-metylating system of isoproterenol by stop-flow ischemia in the perfused rat heart. J Pharmacol Exp Ther 1987;242: 1086–9.
[11] Carlsson L, Abrahamsson T, Almgren O. Release of noradrenaline in myocardial ischemia-importance of local inactivation by neuronal and extraneuronal mechanisms. J Cardiovasc Pharmacol 1986;8:543–53.
[12] Goldstein DS, Katzper M, Linares O, Kopin I. Kinetic model from the fate of 6-[^{18}F]fluorodopamine in the human heart: a novel means to examine cardiac sympathetic neuronal function. Naunyn Schmiedebergs Arch Pharmacol 2002;365:38–49.
[13] Tokunaga N, Yamazaki T, Akiyama T, Sano S, Mori H. In vivo monitoring of norepinephrine and its metabolites in skeletal muscle. Neurochem Int 2003;43:573–80.
[14] Akiyama T, Yamazaki T, Ninomiya I. In vivo monitoring of myocardial interstitial norepinephrine by dialysis technique. Am J Physiol 1991;261:H1643–7.
[15] Le Quellec A, Dupin S, Genissel P, Saivin S, Marchand B, Houin G. Microdialysis probe calibration: gradient and tissue dependent changes in no net flux and reverse dialysis methods. J Pharmacol Toxicol Methods 1995;33:11–6.
[16] Yamazaki T, Akiyama T, Shindo T. Routine high-performance liquid chromatographic determination of myocardial interstitial norepinephrine. J Chromatogr B, Biomed Sci Appl 1995;670:328–31.
[17] Takauchi Y, Kitagawa H, Kawada T, Akiyama T, Yamazaki T. High-performance liquid chromatographic determination of myocardial interstitial dihydroxyphenylglycol. J Chromatogr B, Biomed Sci Appl 1997;693:218–21.
[18] Tokunaga N, Yamazaki T, Akiyama T, Mori H. Detection of 3-methoxy-4-hydroxyphenylglycol in rabbit skeletal muscle microdialysate. J Chromatogr B, Biomed Sci Appl 2003;798:163–6.
[19] Fujii T, Yamazaki T, Akiyama T, Sano S, Mori H. In vivo assessment of catechol *O*-methyltransferase activity in rabbit skeletal muscle. Auton Neurosci 2004;111:140–3.
[20] Winer BJ. Statistical principles in experimental design. 2nd ed. New York: McGraw-Hill; 1971.
[21] Trendelenburg U. The extraneuronal uptake and metabolism of catecholamines in the heart. In: Paton DM, editor. The mechanism of neuronal and extraneuronal transport of catecholamines. 1st ed. New York: Raven Press; 1976. p. 259–80.
[22] Eisenhofer G, Pecorella W, Pacak K, Hooper D, Kopin I. The neuronal and extraneuronal origins of plasma 3-methoxy-4-hydroxyphenylglycol in rats. J Auton Nerv Syst 1994;50:93–107.
[23] Friedgen B, Wolfel R, Russ H, Schömig E, Graefe KH. The role of extraneuronal amine transport systems for the removal of extracellular catecholamine in the rabbit. Naunyn Schmiedebergs Arch Pharmacol 1996;354:275–86.
[24] Goldstein D, Eisenhofer G, Stull R, Joan Folio C, Kaiser HR, Kopin IJ. Plasma dihydroxyphenylgylcol and intraneuronal disposition of norepinephrine in humans. J Clin Invest 1988;81:213–20.
[25] Schömig A, Kurz T, Richardt G, Schömig E. Neuronal sodium homeostasis and axoplasmic amine concentration determine calcium-independent noradrenaline release in normoxic and ischemic rat heart. Circ Res 1988;63:214–26.
[26] Schömig E, Russ H, Staudt K, Martel F, Gliese M, Gründemann D. The extraneuronal monoamine transporter exists in human central nervous system glia. Adv Pharmacol 1998;42:356–9.
[27] Burgdorf C, Dendorfer A, Kurz T, Schömig E, Stolting I, Schutte F, et al. Role of neuronal KATP channels and extraneuronal monoamine transporter on norepinephrine overflow in a model of myocardial low flow ischemia. J Pharmacol Exp Ther 2004;309:42–8.
[28] Kitagawa H, Yamazaki T, Akiyama T, Yahagi N, Kawada T, Mori H, et al. Modulatory effects of ketamine on catecholamine efflux from in vivo cardiac sympathetic nerve endings in cats. Neurosci Lett 2002;324:232–6.
[29] Lundy PM, Frew R. Ketamine potentiates catecholamine responses of vascular smooth muscle by inhibition of extraneuronal uptake. Can J Physiol Pharmacol 1981;59:520–7.
[30] Eisenhofer G. Plasma normetanephrine for examination of extraneuronal uptake and metabolism of noradrenaline in rats. Naunyn Schmiedebergs Arch Pharmacol 1994;349:259–69.
[31] Schömig A. Catecholamine in myocardial ischemia. Systemic and cardiac release. Circulation 1990;82(3 Suppl):II13–22.
[32] Illi A, Sundberg S, Koulu M, Scheinin M, Heinavaara S, Gordin A. COMT inhibition by high-dose entacapone does not affect hemodynamics but changes catecholamine metabolism in healthy volunteers at rest and during exercise. Int J Clin Pharmacol Ther 1994;32:582–8.
[33] Männistö PT, Kaakkola S. Catechol-*O*-methyltransferase (COMT): biochemistry, molecular biology, pharmacology, and clinical efficacy of the new selective COMT inhibitors. Pharmacol Rev 1999;51: 593–628.

β-Adrenoceptor Blocker Carvedilol Provides Cardioprotection via an Adenosine-Dependent Mechanism in Ischemic Canine Hearts

Hiroshi Asanuma, MD, PhD; Tetsuo Minamino, MD, PhD; Shoji Sanada, MD, PhD; Seiji Takashima, MD, PhD; Hisakazu Ogita, MD, PhD; Akiko Ogai, BS; Masanori Asakura, MD, PhD; Yulin Liao, MD; Yoshihiro Asano, MD, PhD; Yasunori Shintani, MD; Jiyoong Kim, MD; Yoshiro Shinozaki, BS; Hidezo Mori, MD, PhD; Koichi Node, MD, PhD; Soichiro Kitamura, MD, PhD; Hitonobu Tomoike, MD, PhD; Masatsugu Hori, MD, PhD; Masafumi Kitakaze, MD, PhD

Background—Carvedilol is a β-adrenoceptor blocker with a vasodilatory action that is more effective for the treatment of congestive heart failure than other β-blockers. Recently, carvedilol has been reported to reduce oxidative stress, which may consequently reduce the deactivation of adenosine-producing enzymes and increase cardiac adenosine levels. Therefore, carvedilol may also have a protective effect on ischemia and reperfusion injury, because adenosine mediates cardioprotection in ischemic hearts.

Methods and Results—In anesthetized dogs, the left anterior descending coronary artery was occluded for 90 minutes, followed by reperfusion for 6 hours. Carvedilol reduced the infarct size (15.0±2.8% versus 40.9±4.2% in controls), and this effect was completely reversed by the nonselective adenosine receptor antagonist 8-sulfophenyltheophylline (45.2±5.4%) or by an inhibitor of ecto-5′-nucleotidase (44.4±3.6%). There were no differences of either area at risk or collateral flow among the various groups. When the coronary perfusion pressure was reduced in other dogs so that coronary blood flow was decreased to 50% of the nonischemic level, carvedilol increased coronary blood flow (49.4±5.6 to 73.5±7.5 mL · 100 g^{-1} · min^{-1}; $P<0.05$) and adenosine release (112.3±22.2 to 240.6±57.1 nmol/L; $P<0.05$) during coronary hypoperfusion. This increase of coronary blood flow was attenuated by either 8-sulfophenyltheophylline or superoxide dismutase. In human umbilical vein endothelial cells cultured with or without xanthine and xanthine oxidase, carvedilol caused an increase of ecto-5′-nucleotidase activity.

Conclusions—Carvedilol shows a cardioprotective effect against ischemia and/or reperfusion injury via adenosine-dependent mechanisms. (***Circulation.*** **2004;109:2773-2779.)**

Key Words: adenosine ■ stress ■ ischemia ■ reperfusion ■ infarction

Beta-adrenoceptor antagonists (β-blockers) are used for the treatment of ischemic heart disease because these drugs reduce adrenergic activity.[1,2] Carvedilol is a β-blocker that has shown efficacy for chronic heart failure in several large-scale trials.[3,4] Carvedilol decreases vascular resistance[3] and improves the pathophysiology of chronic heart failure.[5] This drug dilates both systemic and coronary vessels,[6] which is not a typical characteristic of β-blockers. Although this vasodilatory action may contribute to the beneficial effects of carvedilol in ischemic or nonischemic heart failure,[5] it may not be the primary mechanism of cardioprotection, because vasodilators are not always effective at protecting the heart.[7] Interestingly, carvedilol can also reduce oxidative stress,[8] which causes cellular damage through inactivation of membrane enzymes, pumps, and proteins, such as Na^+/K^+-ATPase,[9] Ca^{2+} channels,[10] and ecto-5′-nucleotidase.[11] Ecto-5′-nucleotidase is the enzyme that produces adenosine, and adenosine is believed to ameliorate chronic heart failure or myocardial ischemia.[12]

To investigate the relationship between the cardioprotective effect of carvedilol and the reduction of oxidative stress on the enhancement of adenosine release, we examined whether carvedilol could reduce infarct size via adenosine- or ecto-5′-nucleotidase–dependent mechanisms in canine hearts. We also investigated whether carvedilol could increase coronary blood flow (CBF) via attenuation of oxidative stress and enhancement of adenosine release in ischemic canine hearts.

Received July 23, 2003; de novo received December 18, 2003; revision received February 18, 2004; accepted February 25, 2004.

From the Department of Internal Medicine and Therapeutics, Osaka University Graduate School of Medicine, Suita (H.A., T.M., S.S., S.T., H.O., M.A., Y.L., Y.A., Y. Shintani, K.N., M.H.); the Cardiovascular Division, National Cardiovascular Center, Suita (A.O., J.K., H.M., S.K., H.T., M.K.); and the Physiology Department, Tokai University School of Medicine, Isehara (Y. Shinozaki), Japan.

Correspondence to Masafumi Kitakaze, MD, Cardiovascular Division, National Cardiovascular Center, 5-7-1 Fujishirodai, Suita City, Osaka Pref. 565-8565, Japan. E-mail kitakaze@zf6.so-net.ne.jp

Circulation **is available at http://www.circulationaha.org** **DOI: 10.1161/01.CIR.0000130917.12959.04**

Methods

Instrumentation

We have previously reported the details of the instrumentation procedure.[13] In brief, hybrid dogs (HBD) mated with the beagle, American fox hound, and Labrador retriever for laboratory use (weighing 15 to 21 kg; Kitayama Labes, Gifu, Japan) were anesthetized by an intravenous injection of sodium pentobarbital (30 mg/kg), intubated, and ventilated with room air mixed with oxygen (100% O_2 at flow rate of 1.0 to 1.5 L/min). The arterial blood pH, Po_2, and Pco_2 before the protocol was begun were 7.38±0.02, 104±3 mm Hg, and 38.7±1.6 mm Hg, respectively. End-diastolic length (EDL) was determined at the R wave on the ECG, and end-systolic length (ESL) was determined at the minimum pressure differential. Then, fractional shortening (FS) was calculated as [(EDL−ESL)/EDL]×100%. Agents were administered into the left anterior descending coronary artery (LAD) via the bypass tube. To constitute the coronary bypass between the carotid artery and the LAD, <30 seconds interruption of the LAD was necessary, but this brief period of ischemia does not provoke either myocardial injury or protection. This study conformed to the *Position of the American Heart Association on Research Animal Use* adopted by the Association in November 1984.

Experimental Protocols

Protocol 1: Effects of Carvedilol on Adenosine Release and CBF in Nonischemic Myocardium

After hemodynamics became stable, coronary arterial and venous blood samples were obtained for the measurement of adenosine concentrations,[11] and the difference between the adenosine levels in coronary arterial and venous blood [VAD(Ado)] was then calculated.

Five HBD dogs were used in protocol 1. Hemodynamic parameters (ie, systolic and diastolic aortic blood pressure and heart rate) were monitored. Carvedilol was infused at 1.5 $\mu g \cdot kg^{-1} \cdot min^{-1}$ (an infusion rate of 0.0167 mL $\cdot kg^{-1} \cdot min^{-1}$ at a concentration of 0.09 mg/mL) for 10 minutes, and then coronary perfusion pressure (CPP), CBF, FS, and VAD(Ado) were measured. Carvedilol was dissolved in a small volume of DMSO (final concentration, <0.15%). In a preliminary study, this dose of carvedilol was shown to be the minimum dose that caused maximal coronary vasodilation in ischemic or nonischemic hearts. We also confirmed that this volume of DMSO did not change either coronary hemodynamics or VAD(Ado) in ischemic or nonischemic hearts.

Protocol 2: Effects of Carvedilol or Propranolol on Adenosine Release and CBF in Ischemic Hearts

After hemodynamics became stable, coronary arterial and venous blood samples were obtained for blood gas analysis and for measurement of adenosine[11,13] and lactate[14] levels. Lactate extraction ratio (LER) was calculated as the coronary arteriovenous difference of the lactate concentration multiplied by 100 and divided by the arterial lactate concentration.

Twenty HBD dogs were used in protocol 2. Hemodynamic parameters were monitored. To examine whether administration of carvedilol caused coronary vasodilation and reduced the severity of myocardial ischemia and whether adenosine-dependent mechanisms are involved in these actions, saline (n=5), α,β-methyleneadenosine diphosphate (AMP-CP) at 80 $\mu g \cdot kg^{-1} \cdot min^{-1}$ (an infusion rate of 0.0167 mL $\cdot kg^{-1} \cdot min^{-1}$ at a concentration of 4.8 mg/mL, n=5), or 8-sulfophenyltheophylline (8-SPT) at 30 $\mu g \cdot kg^{-1} \cdot min^{-1}$ (an infusion rate of 0.0167 mL $\cdot kg^{-1} \cdot min^{-1}$ at a concentration of 1.8 mg/mL, n=5) was infused into the bypass tube. AMP-CP is an inhibitor of ecto-5′-nucleotidase, whereas 8-SPT is a nonspecific adenosine receptor antagonist. Both agents were dissolved in saline before administration. After confirming that systemic and coronary hemodynamics were unchanged for 5 minutes after each drug infusion, CPP was reduced so that CBF decreased to 50% of the baseline level for 5 minutes. Then, infusion of carvedilol was started at 1.5 $\mu g \cdot kg^{-1} \cdot min^{-1}$ (an infusion rate of 0.0167 mL $\cdot kg^{-1} \cdot min^{-1}$ at a concentration of 0.09 mg/mL) and was continued for 10 minutes, while CPP was maintained at the reduced level. A preliminary study showed that the above-mentioned dose of 8-SPT was the minimum dose that prevented coronary vasodilation induced by adenosine at 2 $\mu g \cdot kg^{-1} \cdot min^{-1}$, whereas the dose of carvedilol (1.5 $\mu g \cdot kg^{-1} \cdot min^{-1}$) was the minimum level that caused maximal coronary vasodilation.

In addition, propranolol was infused at 30 $\mu g \cdot kg^{-1} \cdot min^{-1}$ (an infusion rate of 0.0167 mL $\cdot kg^{-1} \cdot min^{-1}$ at a concentration of 1.8 mg/mL) to investigate whether it had effects identical to those of carvedilol (n=5). This dose of propranolol corresponds to 15 μg/mL, and the effective dose of propranolol is >10 μg/mL, indicating that the dose of propranolol in the present study is sufficient to antagonize β-receptors of the hearts.

Protocol 3: Influence of the Antioxidant Activity of Carvedilol on CBF

To examine whether carvedilol eliminates oxidative stress and causes adenosine-dependent coronary vasodilation in ischemic hearts, either saline (an infusion rate of 0.0167 mL $\cdot kg^{-1} \cdot min^{-1}$ at a concentration of 1.5 mg/mL, n=5) or human recombinant superoxide dismutase (SOD) (5340 IU/mg, >99% purity) at 25 $\mu g \cdot kg^{-1} \cdot min^{-1}$ (an infusion rate of 0.0167 mL $\cdot kg^{-1} \cdot min^{-1}$ at a concentration of 1.5 mg/mL, n=5) was infused into the bypass tube. CPP was then reduced so that CBF decreased to 50% of the baseline level for 5 minutes. Subsequently, infusion of carvedilol at 1.5 $\mu g \cdot kg^{-1} \cdot min^{-1}$ (an infusion rate of 0.0167 mL $\cdot kg^{-1} \cdot min^{-1}$ at a concentration of 0.09 mg/mL) was initiated and continued for 10 minutes, while CPP was maintained at the reduced value. As a marker of oxidative stress, the 8-iso-prostaglandin $F_{2\alpha}$ level was measured in coronary arterial and venous blood, and the arteriovenous difference of 8-iso-prostaglandin $F_{2\alpha}$ [VAD(8-Iso-$F_{2\alpha}$)] was calculated. We confirmed that this dose of SOD had no effect on either systemic or coronary hemodynamic parameters.[11]

Protocol 4: Effects of Carvedilol on Infarct Size After 90 Minutes of Ischemia

In HBD dogs, the bypass tube to the LAD was occluded for 90 minutes, followed by reperfusion for 6 hours, together with administration of either saline (n=7, control) or DMSO (0.0167 mL $\cdot kg^{-1} \cdot min^{-1}$, n=5) from 10 minutes before occlusion until 1 hour of reperfusion, except at the time of coronary occlusion. Hemodynamic parameters were monitored during myocardial ischemia and after the start of reperfusion. In the carvedilol group (n=5), carvedilol at 1.5 $\mu g \cdot kg^{-1} \cdot min^{-1}$ (an infusion rate of 0.0167 mL $\cdot kg^{-1} \cdot min^{-1}$ at a concentration of 0.09 mg/mL) was infused from 10 minutes before coronary occlusion until 60 minutes after the start of reperfusion, except during occlusion. In the carvedilol+8-SPT group (n=6) and the carvedilol+AMP-CP group (n=6), the effect of carvedilol was tested during concomitant administration of either 8-SPT at 30 $\mu g \cdot kg^{-1} \cdot min^{-1}$ or AMP-CP at 80 $\mu g \cdot kg^{-1} \cdot min^{-1}$. In the 8-SPT group (n=6) and the AMP-CP group (n=7), 90 minutes of ischemia and 6 hours of reperfusion were performed during treatments with 8-SPT and AMP-CP, respectively. Either 8-SPT or AMP-CP was infused from 10 minutes before coronary occlusion until 60 minutes after the start of reperfusion, except during occlusion. In all groups, infarct size was assessed after 6 hours of reperfusion.

Protocol 5: Effects of Carvedilol on 5′-Nucleotidase Activity

In human umbilical vein endothelial cells (HUVECs) cultured with or without xanthine (1×10^{-4} mol/L) and xanthine oxidase (1.6×10^{-3} U/mL), 5′-nucleotidase activity was measured by an enzyme assay after exposure to carvedilol (0, 1×10^{-8} to 1×10^{-5} mol/L) for 15 minutes.[15]

Analyses

The methods of measuring plasma adenosine levels,[11] myocardial ecto-5′-nucleotidase activity,[11,16] and plasma lactate levels[13] have been reported previously.

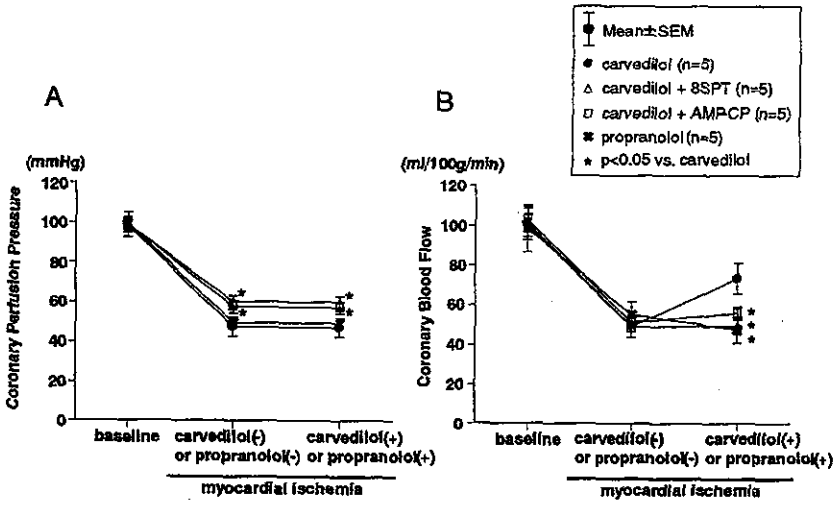

Figure 1. Effects of carvedilol on coronary hemodynamics in ischemic myocardium. A and B show CPP and CBF, respectively. Statistical analysis was performed by ANOVA followed by Bonferroni's test.

Measurement of Infarct Size and Collateral Blood Flow

In protocol 4, the area of myocardial necrosis and the area at risk[16] were measured in all of the dogs upon completion of the protocol by an operator who had no knowledge of the treatment given to each animal. Infarct size was expressed as a percentage of the area at risk.

Regional myocardial blood flow was determined as described previously.[17] Nonradioactive microspheres (Sekisui Plastic Co) made of inert plastic were labeled with bromine. Microspheres were administered at 80 minutes after the start of coronary occlusion. The radio fluorescence of the stable heavy elements was measured with a wavelength dispersive spectrometer (PW 1480, Phillips Co). Because the level of energy emitted is characteristic of specific elements, it was possible to quantify the radio fluorescence of the heavy element with which the microspheres were labeled. Myocardial blood flow was calculated according to the following formula: *time flow=(tissue count)×(reference flow)/(reference count)*, and was expressed in milliliters per minute per gram wet weight. Endomyocardial blood flow was measured at the inner half of the left ventricular wall.

Exclusion Criteria

To ensure that all of the animals used for analysis of infarct size in protocol 4 were healthy and were exposed to a similar extent of ischemia, the following standards were used for exclusion of unsatisfactory dogs: (1) subendocardial collateral blood flow >15 mL · 100 g^{-1} · min^{-1}, (2) a heart rate >170 bpm, and (3) >2 consecutive attempts required to terminate ventricular fibrillation using low-energy DC pulses applied directly to the heart.

Statistical Analysis

Statistical analysis was performed by use of ANOVA[18,19] to compare data among the groups. When ANOVA indicated a significant difference, paired data were compared by use of the Bonferroni test. Changes of the hemodynamic and metabolic parameters over time were assessed by ANOVA with repeated measures. Results were expressed as the mean±SEM, with a value of $P<0.05$ being considered significant.

Results

Effects of Carvedilol on VAD(Ado) in Nonischemic Myocardium

Neither systemic hemodynamic parameters (mean blood pressure, 101.0±2.1 versus 98.6±3.2 mm Hg and heart rate, 130.2±3.7 versus 128.0±3.3 bpm) nor FS (20.1±1.0% versus 21.5±1.0%) changed during the infusion of carvedilol. In contrast, CBF was increased (98.4±8.5 versus 112.6±9.6 mL · 100 g^{-1} · min^{-1}, $P<0.05$), as was VAD(Ado) (40.9±4.0 versus 68.6±5.5 nmol/L, $P<0.05$).

Effects of Either Carvedilol or Propranolol on VAD(Ado) During Coronary Hypoperfusion

Administration of either 8-SPT or AMP-CP did not alter the systemic hemodynamics (mean blood pressure, 98.8±6.1 versus 101.8±5.8 mm Hg before and after 8-SPT and 99.0±3.0 versus 102.0±3.2 mm Hg before and after AMP-CP; heart rate, 132.2±6.9 versus 132.4±6.1 min^{-1} before and after 8-SPT and 131.8±4.6 versus 132.8±3.4 min^{-1} before and after AMP-CP) or the coronary hemodynamic and metabolic parameters (Figures 1 through 3). Before both CBF and CPP were reduced, there were no significant differences in hemodynamic and metabolic parameters among the 3 groups. In untreated dogs, administration of saline did not affect CPP, LER, or FS. However, addition of carvedilol increased VAD(Ado), CBF, LER, and FS, even in the

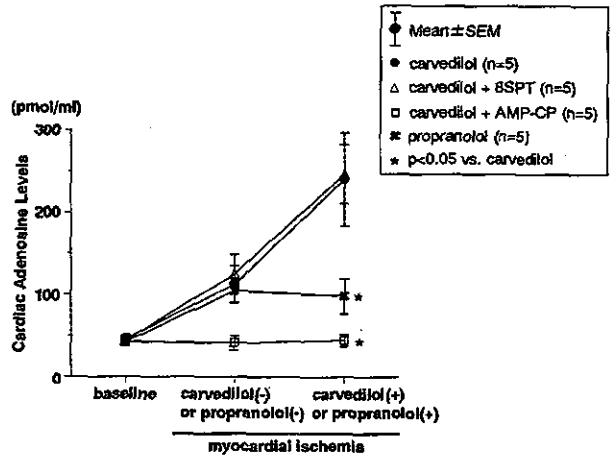

Figure 2. Changes of difference in adenosine levels between coronary venous and arterial blood [VAD(Ado)] in ischemic myocardium. Carvedilol increased VAD(Ado), which was attenuated by an ecto-5'-nucleotidase inhibitor. Statistical analysis was performed by ANOVA followed by Bonferroni's test.